4
Micromixing Devices

4.1
Role of Mixing for the Performance of Chemical Reactors

Mixing is one of the basic unit operations involved in chemical transformations. The problems associated with bad mixing may have a decisive impact on the product distribution and the performance of a chemical reactor. Mixing is a general definition applied for different physical processes. It can be subdivided into two main classes:

1) Microscopic mixing: mixing of individual molecules, like homogenization of two miscible fluids, or dissolution of a solid in a liquid without the formation of any concentration (temperature) gradients.
2) Macroscopic mixing: mixing of groups or aggregates of molecules, such as
   a. Suspension of a solid in a liquid or slurry formation
   b. Dispersion (or emulsification) of two immiscible liquids
   c. Dispersion of a gas in a liquid (or foam formation).

In general, good mixing at the macroscopic scale can be easily attained, but it is much more difficult to obtain an intimate mixing on the molecular scale. Nonuniform reactant concentrations on the molecular scale may have a significant influence on the effective transformation rate and the product distribution, especially when complex and rapid chemical reactions are involved. In this chapter we mainly consider the microscopic mixing between miscible fluids. This means that two completely miscible reacting fluids are brought together. If the characteristic mixing time defined as the time required for two fluids to become homogenous on the molecular scale is in the same order of magnitude as the characteristic reaction time or even longer, the product distribution is strongly affected, especially in the case of complex networks with parallel and/or consecutive reactions [1, 2]. To avoid the negative effect on reactor productivity and yield of the desired product (often an intermediate in a complex reaction network), the characteristic mixing time should be at least 10-fold shorter than the characteristic reaction time.

To describe the mixing process and its influence on the performance of chemical reactors, different models were developed [3, 4]. Herein we discuss the influence of the micromixing process using the concept of segregation as proposed by Baldyga

Microstructured Devices for Chemical Processing, First Edition.
Madhvanand N. Kashid, Albert Renken and Lioubov Kiwi-Minsker.

[5]. In addition, we restrict the discussion to ideal tubular reactors supposing plug flow behavior.

The concept of segregation in chemical reactors was first introduced by Danckwerts in 1953 [6]. He defined an intensity of segregation, $I_{s,}$ varying between one and zero. For $I_s = 0$, complete mixing on the molecular scale is attained. The situation of complete segregation is illustrated in Figure 4.1. It shows a system with two reactants A_1 and A_2, which are initially present in two separated volumes (expressed as volumetric fractions). Segregation also may be observed in tubular reactors with separate feeds of the reacting fluids (Figure 4.2).

Danckwerts defined the intensity of segregation in turbulent flow, I_s, in terms of the mean square of the concentration fluctuation as shown in Figure 4.3 and given in Equation 4.1.

$$I_s = \frac{\overline{\Delta c_1^2}}{\left(\overline{\Delta c_1^2}\right)_0} \tag{4.1}$$

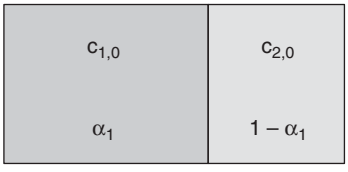

Figure 4.1 Complete segregation ($I_s = 1$) of reactants A_1 and A_2 in two volume fractions.

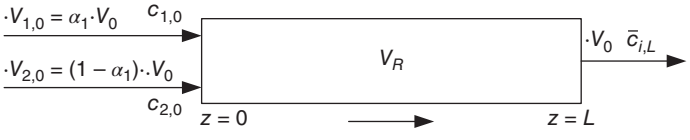

Figure 4.2 Feeding of unmixed reactants to a tubular reactor. Constant fluid density.

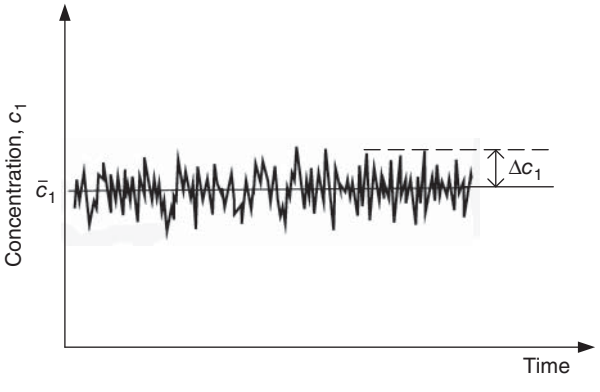

Figure 4.3 Time-variant concentration fluctuations around the mean value $\bar{c}_1$. (Reproduced from Ref. [5]. Copyright © 2013, Wiley-VCH GmbH & Co. KGaA.)

where $(\overline{\Delta c_1^2})_0$ corresponds to the initial mean square of concentration fluctuations. The mean square of the concentration variations is given in Equation 4.2

$$\overline{\Delta c_1^2} = \overline{(c_1 - \overline{c_1})^2} \tag{4.2}$$

For the situation shown in Figure 4.1 the initial mean square fluctuations are given by

$$(\overline{\Delta c_1^2})_0 = c_{1,0}^2 \cdot \alpha_1(1 - \alpha_1) \tag{4.3}$$

For separate feed to a continuously operated reactor, the volume fraction α_1 corresponds to the volumetric flow containing A_1 referred to the total inlet flow.

$$\alpha_1 = \frac{\dot{V}_{1,0}}{\dot{V}_{1,0} + \dot{V}_{2,0}} = \frac{\dot{V}_1}{\dot{V}_0} \tag{4.4}$$

Depending on the mixing intensity in the reactor, the segregation will diminish with increasing residence time. The rate of decay of the concentration variance can be supposed to be a first order process as indicated in Equation 4.5

$$r_d = -b_s \cdot \overline{\Delta c_1^2} = -\frac{1}{t_{mx}} \cdot \overline{\Delta c_1^2} \tag{4.5}$$

The parameter b_s is equivalent to the inverse mixing time, t_{mx}, and is a function of the power dissipation per volume and the geometry of the mixing device.

In plug flow reactors (PFRs) under steady state, the segregation intensity will decay with the distance from the reactor inlet, respectively, with the residence time, τ.

$$\frac{\overline{\Delta c_1^2}}{\left(\overline{\Delta c_1^2}\right)_0} = I_s = \exp(-b_s\tau) = \exp(-b_s\tau_{PFR}Z)$$
$$\text{with } \tau_{PFR} = V_R/\dot{V}_0;\ Z = V/V_R = z/L \text{ (constant diameter)} \tag{4.6}$$

The transformation rate of an irreversible second order reaction in a partially segregated fluid can be expressed in terms of the mean concentrations and the concentration fluctuations of the reactants [7].

$$\overline{R}_1 = -k \cdot c_1 c_2 = -k \cdot (\overline{c}_1 \cdot \overline{c}_2 + \overline{\Delta c_1 \Delta c_2})$$
$$\frac{d\overline{c}_1}{d\tau} = \overline{R}_1 = -k \cdot (\overline{c}_1 \cdot \overline{c}_2 - I_s \overline{c}_{1,0} \cdot \overline{c}_{2,0})$$
$$\text{with : } \overline{\Delta c_1 \Delta c_2} = -I_s(\overline{c}_{1,0} \cdot \overline{c}_{2,0}) \tag{4.7}$$

With the following dimensionless variables:

$M = \overline{c}_{2,0}/\overline{c}_{1,0}$, $f_i = \overline{c}_i/\overline{c}_{1,0}$, $\overline{c}_{2,0} = c_{2,0} \cdot (1 - \alpha_1)$; $\overline{c}_{1,0} = c_{1,0} \cdot \alpha_1$, $DaI = k\overline{c}_{1,0}\tau_{PFR}$

The material balance for the reactant A_1 can be expressed in dimensionless form as follows:

$$\frac{df_1}{dZ} = -DaI \cdot [f_1 \cdot (f_1 + M - 1) - I_s M] \tag{4.8}$$

For given reaction conditions and residence time in a PFR, the axial concentration profile and the outlet conversion depends strongly on the ratio between mixing time and characteristic reaction time. This ratio can be interpreted as a second Damköhler number for mixing $DaII_{mx}$.

$$DaII_{mx} = \frac{t_{mx}}{t_r} = k \cdot \bar{c}_{1,0} \cdot t_{mx} \quad \text{(second order reaction)} \tag{4.9}$$

This is shown in Figure 4.4, where the residual concentration of A_1 is plotted as function of the reactor length for different values of $DaII_{mx}$ and constant DaI and equimolar reactant feed ($M = 1$). Whereas for immediate mixing of the reactants at the reactor entrance ($DaII_{mx} = >0$) the conversion of A_1 corresponds to $X = 0.833$ ($f_1 = 0.167$) at $DaI = 5$, the conversion drops to $X = 0.345$ ($f_1 = 0.655$) for $DaII_{mx} = 5$. A roughly four times higher residence time in the reactor is needed to get the same conversion as for $DaII_{mx} = 0$. In general, long mixing times as compared to the characteristic reaction time diminish the reactor performance for reactions with positive reaction orders ($n > 0$). This leads to the increased reactor size in order to attain the same degree of conversion.

Even more important is the influence of slow mixing on the performance of complex reactions. If the reaction between two fluids takes place to an appreciable extent before the homogeneity is attained, segregation can affect product distribution. This is discussed for consecutive competing reactions represented by Equation 4.10.

$$\begin{aligned} A_1 + A_2 &\xrightarrow{k_1} A_3 \\ A_3 + A_2 &\xrightarrow{k_2} A_4 \end{aligned} \tag{4.10}$$

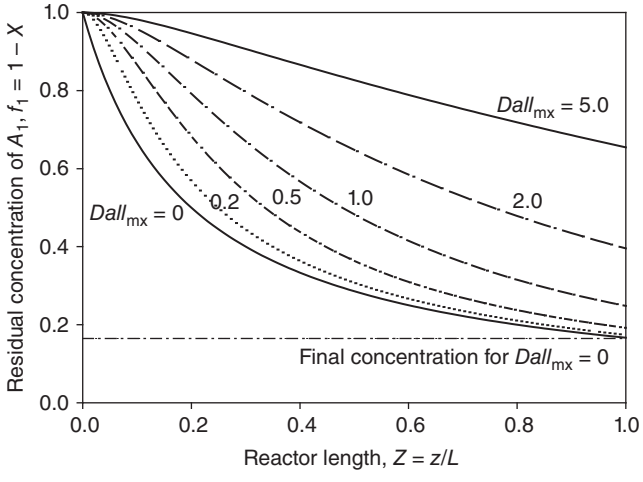

Figure 4.4 Estimated residual concentration of A_1 as function of reactor length for different $DaII_{mx}$. $DaI = 5$; $M = 1$.

Examples of such consecutive competing reactions are chlorination, nitration of hydrocarbons, or the addition of alkene oxides (e.g., ethylene oxide) to amines or alcohols. If the mixing is fast enough, so that the reacting fluid is homogenous before the reaction takes place, the maximum yield of the desired intermediate A_3 will be controlled by the ratio of k_2/k_1. Let us suppose irreversible second order reactions, so the following relations describe the transformation rates of the involved reactants.

$$\begin{aligned} R_1 &= -k_1 \cdot c_1 c_2 \\ R_2 &= -k_1 \cdot c_1 c_2 - k_2 \cdot c_2 c_3 \\ R_3 &= k_1 \cdot c_1 c_2 - k_2 \cdot c_2 c_3 \\ R_4 &= k_2 \cdot c_2 c_3 \end{aligned} \tag{4.11}$$

In batch or ideal PFR the concentration of the intermediate product A_3 will first increase with increasing residence time, pass through a maximum, and finally disappear at long residence times, if the initial reaction partners are fed in stoichiometric ratios. For the simple reaction scheme shown by Equation 4.10, $M = c_{2,0}/c_{1,0}$ must be $M = 2$ for complete transformation of A_1 and A_2. The concentration profiles can be calculated by solving the corresponding mass balances. For a PFR the following mass balances are obtained:

$$\begin{aligned} -\frac{\mathrm{d}c_1}{\mathrm{d}\tau} &= k_1 \cdot c_1 c_2 \\ -\frac{\mathrm{d}c_2}{\mathrm{d}\tau} &= k_1 \cdot c_1 c_2 + k_2 c_2 c_3 \\ \frac{\mathrm{d}c_3}{\mathrm{d}\tau} &= k_1 \cdot c_1 c_2 - k_2 c_2 c_3 \\ \frac{\mathrm{d}c_4}{\mathrm{d}\tau} &= k_2 c_2 c_3 \end{aligned} \tag{4.12}$$

Initial conditions: $\tau = 0 : \quad c_1 = c_{1,0}; \quad c_2 = c_{2,0}; \quad c_3 = c_4 = 0$

By dividing the third equation by the first one, the residence time can be eliminated and we get a relationship between the reactant concentrations.

$$-\frac{\mathrm{d}c_3}{\mathrm{d}c_1} = 1 - \frac{k_2}{k_1} \cdot \frac{c_3}{c_1} \tag{4.13}$$

After integration, a relation between the yield of the intermediate A_3 and the conversion of the key component A_1 is obtained.

$$\begin{aligned} Y_{3,1} &= \frac{(1-X)^{\kappa} - (1-X)}{1-\kappa}; \quad \kappa = \frac{\mathrm{k_2}}{\mathrm{k_1}} \neq 1 \\ Y_{3,1} &= (X-1) \cdot \ln(1-X); \quad \kappa = \frac{\mathrm{k_2}}{\mathrm{k_1}} = 1 \end{aligned} \tag{4.14}$$

The intermediate yield as function of conversion is dependent only on the ratio of rate constants. This is also true for the maximum attainable yield $Y_{3,1}$.

$$Y_{3,1,\max} = \kappa^{\frac{\kappa}{1-\kappa}}, \quad \kappa = \frac{k_2}{k_1} \neq 1$$
$$Y_{3,1,\max} = \frac{1}{\exp(1)} = 0.368, \quad \kappa = \frac{k_2}{k_1} = 1 \tag{4.15}$$

Decreasing the ratio of the rate constants leads to higher maximum yield of the intermediate, and the maximum value is shifted to higher reactant conversion as illustrated in Figure 4.5. For understoichiometric ratio of the reactants ($M < 2$), A_1 cannot be completely converted and the final yield and conversion is indicated by the intersection of the dashed lines with the corresponding curve (Figure 4.5).

The transformation rates in terms of the intensity of segregation and mean concentrations are given by neglecting the influence of the covariance $\overline{\Delta c_2 \cdot \Delta c_2}$ [8]:

$$\overline{R}_1 = -k_1 \cdot (\overline{c}_1 \cdot \overline{c}_2 + \overline{\Delta c_1 \Delta c_2})$$
$$\overline{R}_2 = -k_1 \cdot (\overline{c}_1 \cdot \overline{c}_2 + \overline{\Delta c_1 \Delta c_2}) - k_2 \cdot \overline{c}_2 \cdot \overline{c}_3$$
$$\overline{R}_3 = k_1 \cdot (\overline{c}_1 \cdot \overline{c}_2 + \overline{\Delta c_1 \Delta c_2}) - k_2 \cdot \overline{c}_2 \cdot \overline{c}_3$$
$$\overline{R}_4 = k_2 \cdot \overline{c}_2 \cdot \overline{c}_3 \tag{4.16}$$

If the reactant A_1 and A_2 are fed separately to the PFR and mixing is slow as compared to the chemical transformation, significant yield losses for the intermediate product A_3 can be expected, whereas the formation of the final product A_4 will increase. The effect will become more pronounced by increasing the mixing time referred to the characteristic reaction time, which corresponds to $DaII_{\mathrm{mx}} = k_1 \cdot \overline{c}_{1,0} \cdot t_{\mathrm{mx}}$. In Figure 4.6 the influence of $DaII_{\mathrm{mx}}$ on the intermediate

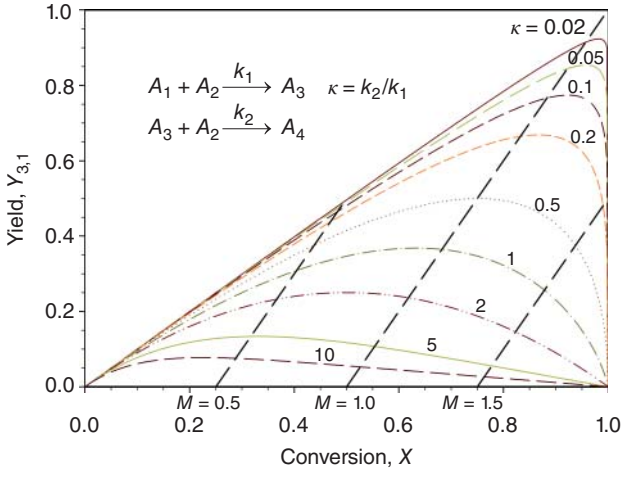

Figure 4.5 Yield of the intermediate product A_3 as a function of conversion and the ratio of the rate constants, κ.

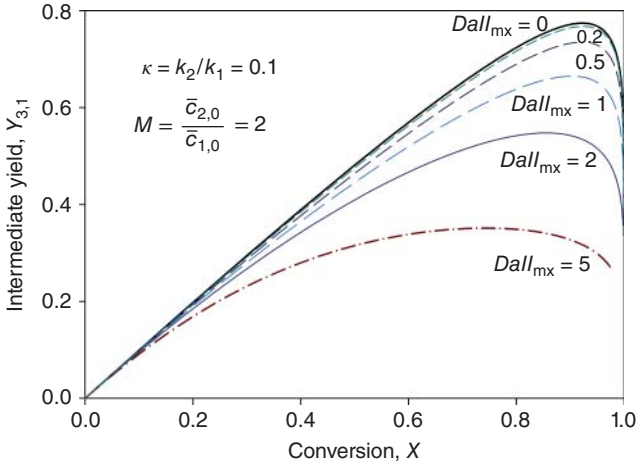

Figure 4.6 Yield of the intermediate product A_3 as a function of conversion for different dimensionless mixing times ($DaII_{mx} = t_{mx}/t_r$); $M = 2$.

A_3 yield as a function of the residence time, respectively, the first Damköhler number, is illustrated for $\kappa = k_2/k_1 = 0.1$ as an example.

In summary, with increasing mixing time as compared to the characteristic reaction time, the maximum yield of the desired intermediate is significantly diminished and shifted to longer residence times, respectively, to higher *DaI* values. At the same time the maximum yield is attained at lower reactant conversion (Figure 4.7). The consequence is a drastic decrease of the reactor performance concomitant with an increased formation of the unwanted by-product, which is often considered as waste.

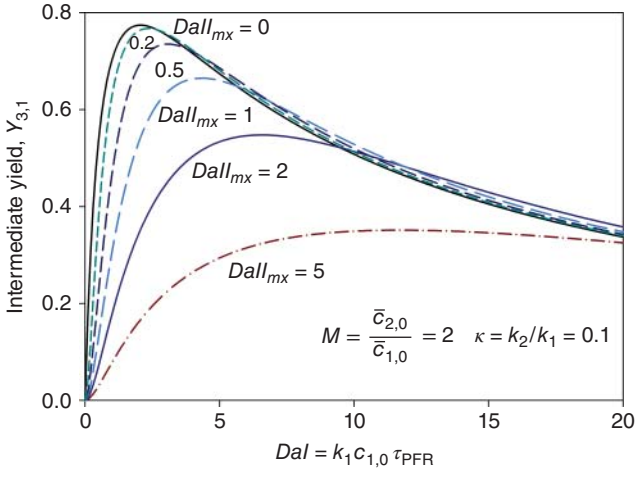

Figure 4.7 Yield of the intermediate product A_3 as function of the dimensionless time (*DaI*) for different dimensionless mixing times ($DaII_{mx} = t_{mx}/t_r$).

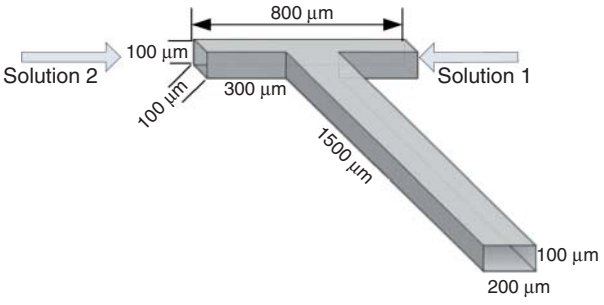

Figure 4.8 T-shaped micromixer [14]. (Adapted with permission from Wiley.)

4.2 Flow Pattern and Mixing in Microchannel Reactors

Microchannel reactors are characterized by small hydraulic diameters of $d_h < 1$ mm. Therefore, laminar flow with Reynolds numbers $Re < 2000$ prevails in microchannels. But, in spite of the laminar flow, vortices and engulfment processes may develop and promote greatly the mixing process. Extensive theoretical and experimental studies of the flow pattern and mixing efficiency in T-shaped micromixer [9–14] confirm that only in smooth channels and at low *Re* less than roughly 100, a stratified flow is formed. The studies were carried out with a T-mixer as shown in Figure 4.8. Within the stratified flow regime, separately fed miscible solutions flow side by side and the mass transfer perpendicular to the main flow direction is controlled by molecular diffusion only. In consequence, the mass transfer is very slow because of the rather thick liquid layers corresponding to half of the channel height.

The spatial structure of the parallel flow of pure water and water colored with rhodamin is illustrated in Figure 4.9. The concentration profile is measured by confocal laser scanning microscopy [14].

Figure 4.9 Parallel flow in a T-mixer ($200 \times 100 \times 100$ mm) system water/water rhodamin, $T = 20\,^{\circ}\mathrm{C}$, $Re = 120$ [14]. (Adapted with permission from Wiley.)

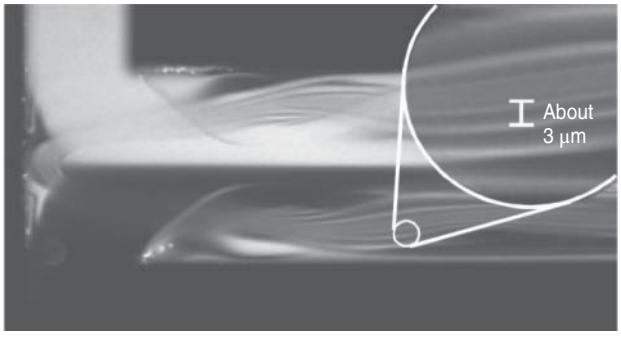

Figure 4.10 Parallel flow in a T-mixer (200 × 100 × 100 mm) system water/water rhodamin, $T = 20\,°C$, $Re = 240$ [14]. (Adapted with permission from Wiley.)

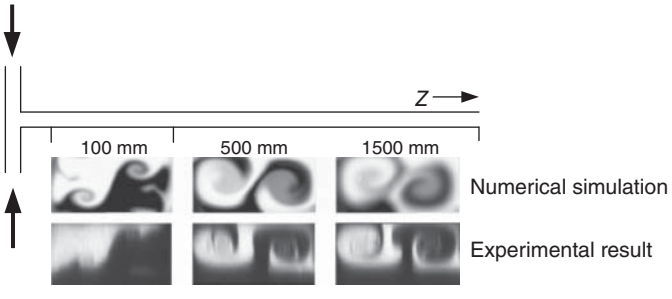

Figure 4.11 Specific interphasial area at different distances from the mixing point. $Re = 186$ [14]. (Adapted with permission from Wiley.)

For higher *Re* the "engulfment regime" sets in. Two different vortices develop within the different layers as seen in Figure 4.10. The stretching and thinning liquid lamellae and the wrapping of lamellae downstream from the mixing point yield in an enlarged interfacial area between the liquids. In this flow regime, fluid elements penetrate in the form of small lamellae of several µm thicknesses in the opposite parts of the channel. This, in turn, greatly improves the mass transfer rate.

The development of the specific contact area along the mixing channel is shown in Figure 4.11. Tracer profiles obtained by numerical simulation for different distances from the mixing point are compared with experimental results [14].

4.3 Theory of Mixing in Microchannels with Laminar Flow

The mixing in a microchannel takes place by diffusion and convection depending on the flow pattern and the operating conditions used [15, 16]. The final mixing on the molecular scale, where the reaction takes place, occurs only by molecular diffusion. The time for diffusion in an elementary structure is defined as

follows [3]:

$$t_D = A' \frac{\left(\frac{l}{2}\right)^2}{D_m} \tag{4.17}$$

with l the thickness of the aggregate, D_m – the molecular diffusion coefficient, and A' – a shape factor.

$$A' = \frac{1}{(p+1)(p+3)}; p = 0(\text{slab}), p = 1\,(\text{cylinder}), p = 2\ (\text{sphere}) \tag{4.18}$$

In liquids, the value of molecular diffusion coefficient is $\sim D_m = 10^{-9}\ \text{m}^2\ \text{s}^{-1}$. In consequence, mixing by diffusion in liquids is a very slow process.

In the case of very low *Re* (<100), a segregated flow is observed in smooth microchannels and mixing occurs by molecular diffusion. In microchannels with stratified flow and diameters of $d_h = 100$ µm, the characteristic time of diffusion is in the order of a second, which is by far too long for fast chemical reactions with characteristic reaction times less than a second.

Under these conditions the mixing process can be promoted only by the reduction of the diffusion distances. Thus, the characteristic dimension (the diameter of the channel) directly influences the micromixing time, that is, the time necessary to achieve mixing on a molecular level by diffusion (Equation 4.17).

Equation 4.17 enables one to estimate the mixing time. The choice of the characteristic dimension in more complex geometry is rather difficult because of multiple laminar vertices, which deform the layers along the three dimensions of space [17]. However, in the case of single-channel micromixers without any complex internal structures, the characteristic dimension can be assumed to be equal to its diameter ($l = d_h$). Mixing in T-mixers at low Re-numbers with stratified flow is discussed in Example 4.1 and 4.2.

Example 4.1: Mixing in stratified laminar flow.

Investigate and plot the mixing time as a function of micromixer diameters in the range of 10 – 1000 µm considering rectangular and cylindrical shapes assuming stratified flow. The diffusion coefficient in the liquid is assumed to be $D_m = 10^{-9}\ \text{m}^2\ \text{s}^{-1}$.

Answer:

The mixing time is estimated based on Equations 4.17 and 4.18 (Figure 4.12):

$$\text{Rectangular channel}: \quad t_{\text{mx}} = t_D = A' \frac{(d_h/2)^2}{D_m}; A' = \frac{1}{3}\ (\text{rectangular channel})$$

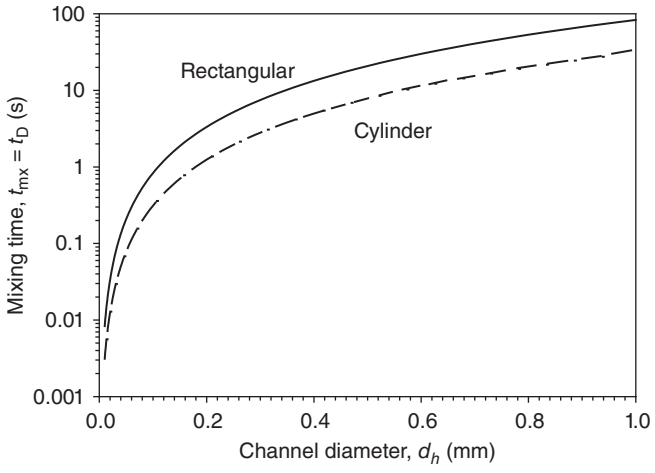

Figure 4.12 Diffusion time for liquid phase in rectangular and cylindrical channels.

Example 4.2: Design of a T-mixer

The liquid phase hydrolysis of ethyl acetate can be described by a second order kinetics

$$\underset{A_1}{CH_3COOCH_2CH_3} + \underset{A_2}{NaOH} \xrightarrow{k} \underset{A_3}{CH_3COONa} + \underset{A_4}{CH_3CH_2OH} \qquad -R_1 = k \cdot c_1 \cdot c_2$$

The reaction rate constants for different temperatures are given as follows [18]:

T (K)	303	313	323	333	343
k (l·(mol s)$^{-1}$)	0.19	0.35	0.58	1.01	1.6

Estimate the hydraulic diameter of a square microchannel reactor to avoid mass transfer influence supposing segregated laminar flow ($Re < 10$). The mean inlet concentration of the reactants is $c_{1,0} = c_{2,0} = 0.4\ \text{mol l}^{-1}$ and the reactor is operated at 303 and 323 K. Both reactants are fed to a T-mixer separately. The diffusion coefficient is $D_m = 10^{-9}\ \text{m}^2\ \text{s}^{-1}$, the kinematic viscosity is $\nu = 10^{-6}\ \text{m}^2\ \text{s}^{-1}$. Determine the residence time for a conversion of $X = 0.9$.

Solution:

The characteristic reaction time is defined as

$t_r = \frac{1}{kc_{1,0}}$ – for a second order reaction.

On the basis of the rate constants measured, the following characteristic reaction times result:

T (K)	303	313	323	333	343
t_r (s)	13.2	7.14	4.31	2.48	1.56

To avoid the influence of mixing on the reaction kinetics, the mixing time should be at least 10-fold shorter than the characteristic reaction time ($DaII_{\mathrm{mx}} \leq 0.1$).

Reaction temperature $T = 303$ K:

$t_{\mathrm{mx}} = 1.3$ s. With $A' = 1/3$ we obtain with Equation 4.17 $d_h = 125$ µm.

Supposing plug flow pattern within the microchannel, for the conversion of 0.9, the residence time can be calculated: $X = \frac{DaI}{1+DaI} = 0.9; DaI = \frac{\tau_{\mathrm{PFR}}}{t_r} = 10 \Rightarrow \tau_{\mathrm{PFR}} = 132\,\mathrm{s}$.

Reaction temperature $T = 323$ K: $t_{\mathrm{mx}} = 0.43$ s; $d_h = 70$ µm; $\tau_{\mathrm{PFR}} = 43$ s.

Reaction temperature $T = 343$ K: $t_{\mathrm{mx}} = 0.16$ s; $d_h = 44$ µm; $\tau_{\mathrm{PFR}} = 16$ s.

In laminar shear flow at $Re >$ ca. 100 the dimension of the characteristic fluid structure decreases in the direction orthogonal to the elongation as discussed in Section 4.2. Therefore, diffusion and convection contribute simultaneously to the mixing process. As diffusion is slow, convection is the dominant process for large structures, and diffusion becomes the controlling step of mixing at small scale. To estimate the overall mixing time, t_{mx}, of intertwined lamellae the following relation is proposed [19]:

$$t_{\mathrm{mx}} = t_{D+\mathrm{shear}} = \frac{1}{2\dot{\gamma}} \operatorname{arcsinh}\left(\frac{0.76 \cdot \dot{\gamma} \cdot 2\delta_0^2}{D_m}\right) \tag{4.19}$$

where δ_0 is the original thickness of the lamella and $\dot{\gamma}$ is the shear rate.

The mean shear rate in laminar flow depends on the kinematic viscosity, ν of the fluid, and the specific power dissipation, ε, expressed in W kg^{-1}:

$$\dot{\gamma} = \left(\frac{\varepsilon}{2\nu}\right)^{\frac{1}{2}} \tag{4.20}$$

The specific power dissipation is proportional to the flow rate and the pressure drop. The pressure drop through open channels with laminar flow is given by the Hagen-Poiseuille equation [20]:

$$\Delta p = 32\zeta \frac{\mu \overline{u}}{d_t^2} L_t \tag{4.21}$$

where ζ is a geometric factor, which is 1 for circular tubes and it depends on the height (H) to width (W) ratio for rectangular channels. The correction factor becomes 0.89 for quadratic channels and assumes the asymptotic value 1.5

when the ratio goes to zero, which corresponds to parallel plates. An empirical correlation is given by the following expression [21]:

$$\zeta = 0.8735 + 0.6265 \exp\left(-3.636 \frac{H}{W}\right) \tag{4.22}$$

It follows for the specific power dissipation:

$$\varepsilon = \frac{\dot{V} \cdot \Delta p}{\rho \cdot V} = \frac{32 \cdot \nu \cdot u^2}{d_t^2} \quad \text{(circular channel)} \tag{4.23}$$

If the thickness of the lamella corresponds initially to the half diameter of the microchannel, we obtain the following relationship for the characteristic mixing time [17]:

$$t_{\mathrm{mx}} = \frac{d_t}{8 \cdot u} \operatorname{arcsinh}(0.76 \cdot Pe) = \frac{d_t^2 / D_m}{8 \cdot Pe} \operatorname{arcsinh}(0.76 \cdot Pe)$$
$$\text{with the Péclet number}: \quad Pe = Re \cdot Sc = \frac{u \cdot d_t}{D_m} \tag{4.24}$$

For $Pe > 20$ the arcsinh $(0.76 \cdot Pe)$ can be replaced by $\ln(1.52 \cdot Pe)$ and Equation 4.24 becomes:

$$t_{\mathrm{mx}} = \frac{d_t^2 / D_m}{8 \cdot Pe} \ln(1.52 \cdot Pe) = \frac{1}{\sqrt{2}} \left(\frac{\nu}{\varepsilon}\right)^{\frac{1}{2}} \ln(1.52 \cdot Pe) \tag{4.25}$$

On the basis of Equation 4.25, the mixing time in microchannels with different diameters between 50 and 1000 µm was estimated to be a function of the specific power dissipation. Physical properties correspond to water at room temperature and atmospheric pressure. Because of the damping effect of the logarithmic function, the influence of the *Pe*-number diminishes and the mixing time can be estimated with the simplified relation in Equation 4.26 (see Figure 4.13).

$$t_{\mathrm{mx}} \cong 0.0075 \cdot \varepsilon^{-0.5} \,\text{(water)} \tag{4.26}$$

The constant in the above equation possess an unit of $\mathrm{m} \cdot \mathrm{s}^{-0.5}$. The mixing characteristics of many different microstructured mixers were studied by using the well-known "Villermaux-Dushman" reaction that takes place in aqueous solutions as described in [22]. The numerous published results collected by Falk and Commenge are added to Figure 4.13. In spite of the large scatter of the experimental results, it can be concluded that for all micromixers the obtainable mixing time seems to depend only on power dissipation. The construction geometry of the mixing device is of minor importance, if at all. It is also evident from the comparison with theoretical predictions that the experimentally observed mixing times are more than 1 order of magnitude longer. The experimental results can be roughly represented by the following relation:

$$t_{\mathrm{mx}} \cong 0.21 \cdot \varepsilon^{-0.5} \,\text{(water)} \tag{4.27}$$

The constant has unit of $\mathrm{m} \cdot \mathrm{s}^{-0.5}$. This corresponds to an energy efficiency of 3–4% (explained in section 4.6). In Example 4.3 the characteristic mixing time is estimated supposing engulfment flow.

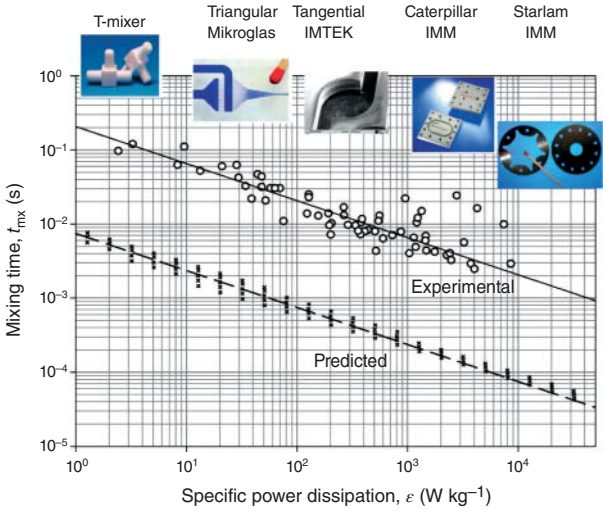

Figure 4.13 Predicted (Equation 4.25) and experimentally determined mixing time as function of the specific power dissipation. (Experimental values taken from Ref. [15]. Adapted with permission from Elsevier.)

The mixing in microchannels with laminar flow in the engulfment regime (validity of Equations 4.19 and 4.24) is summarized as

- Energy dissipation seems to be the only relevant parameter to be taken into consideration for a design of the efficient mixer.
- Multilamination improves mixing by reducing the striation thickness, requires additional mechanical power to create fine multilamellae before contacting.
- It is common that flow fields and concentration fields do not match. Mechanical energy is used to create a flow in the devices, but in zones of pure component with no interface with another component, mechanical energy does not contribute to mixing.

Example 4.3: Mixing time in the engulfment regime.

Estimate the mixing time and the specific power dissipation in a cylindrical channel with a diameter of $d_t = 1\,\text{mm}$, a linear velocity of $u = 0.2\,\text{m} \cdot \text{s}^{-1}$. $D_m = 10^{-9}\,\text{m}^2\,\text{s}^{-1}$, $\nu = 10^{-6}\,\text{m}^2\,\text{s}^{-1}$. Calculate the mixing time and specific power dissipation for a channel with $d_t = 0.5\,\text{mm}$ supposing the same volumetric flow.

Solution:

$$d_t = 1\,\text{mm}: \varepsilon = \frac{\dot{V} \cdot \Delta p}{\rho \cdot V} = \frac{32 \cdot \nu \cdot u^2}{d_t^2}\,(\text{circular channel}) \Rightarrow \varepsilon = 1.3\,\text{W kg}^{-1}; t_{\text{mx}} = 0.18\,\text{s}$$

$$d_t = 0.5\,\text{mm}: \varepsilon = 82\,\text{W kg}^{-1}; t_{\text{mx}} = 0.023\,\text{s}.$$

4.4
Types of Micromixers and Mixing Principles

As presented before, short radial diffusion lengths decrease the mixing time in microchannels even at low flow rates in the laminar flow regime. The mixing time can further be reduced using convective mixing by creating eddies. The convective diffusion enhancement is commonly employed in mixing devices using various methods. A lot of efforts have been made to develop efficient micromixers, and different mixer concepts have been proposed [23, 24]. In general, two types of mixers can be distinguished: passive and active mixers. The former works essentially with energy provided by pumping while the latter uses an external energy source such as acoustic fields, electric fields (electrokinetic instability), or microimpellers. Compared with active micromixers, passive mixers have the advantages of low cost, and easy integration in the microfluidic systems, no complex control units, and no additional power input.

For chemical reactions, micromixers are mounted in front of a residence time unit that provides the required residence time for the reaction to complete. The choice of the micromixer to be used depends on the characteristic reaction time. The mixing time should be at least 10 times shorter compared to the reaction time to avoid losses in reactor performance and product selectivity as discussed in Section 4.1. Besides mixing efficiency, heat transfer potential is an important issue for fast exothermic reaction as is discussed in Chapter 5.

A series of micromixers with different types of mixing elements have been developed using different mixing principles as listed in Table 4.1 and depicted in Figure 4.14. In the case of passive mixing, the flow that is caused by pumping or hydrostatic potential is restructured in order to get faster mixing. Thin lamellae are created in special feed arrangements, termed *interdigital*. A commonly used method to enhance passive mixing in microchannels is to distribute the flow into compartments and reduce diffusion paths beyond the geometric dimensions of the mixing microchannel. For instance, splitting and recombining the feed streams or the injection of substreams via a special microstructure can break the laminar profile and better mixing can be achieved [25]. Chaotic mixing

Table 4.1 Passive and active mixing techniques used in micromixers.

Passive mixing	Active mixing
Interdigital multilamellae arrangements	Ultrasound
Split-and-recombine concepts (SAR)	Acoustically induced vibrations
Chaotic mixing by eddy formation and folding	Electrokinetic instabilities
Droplet binding in two-phase environment	Periodical variation of pressure field
Nozzle injection in flow	Electrowetting-induced joint of droplets
Specialties, e.g., Coanda effect	Magnetohydrodynamic action
	Small impellers
	Piecoelectrically vibrating membrane
	Integrated micro valves/pumps

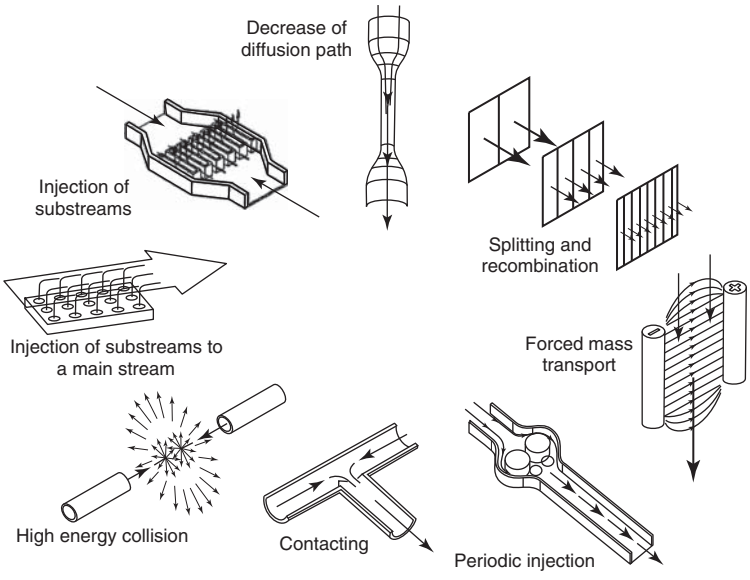

Figure 4.14 Schematic representation of selective passive and active mixing principles used in micromixers [26]. (Adapted with permission from the authors.)

creates eddy-based flow patterns that provide high specific interfaces, though they pose a danger of being spatially inhomogenous. Besides, the injection of many substreams, for example, via nozzles, into one main stream and collision of jets provides a means for turbulent mixing. Finally, a number of specialty flow guidance has been described as, for example, the Coanda effect, relying on a microstructure for redirecting the flow. In the case of active mixers, external energy sources such as ultrasound, acoustic, bubble-induced vibrations, electrokinetic instabilities, periodic variation of flow rate, electrowetting-induced merging of droplets, piezoelectric vibrating membranes, magnetohydrodynamic action, small impellers, integrated microvalves/pumps are used.

4.4.1 Passive Micromixer

4.4.1.1 Single-Channel Micromixers

The simplest passive mixers are often used for characterizing mixing under well-defined conditions (typical geometries are shown in Figure 4.15). If a T-mixer is considered, three flow regimes are observed (Section 4.2):

Stratified flow: a clear interface separates the two flows (lamination) and mixing occurs entirely by diffusion
Vortex flow: the vortex creates secondary surface area
Engulfment flow: the axial symmetry of the flow breaks up (see Section 4.2).

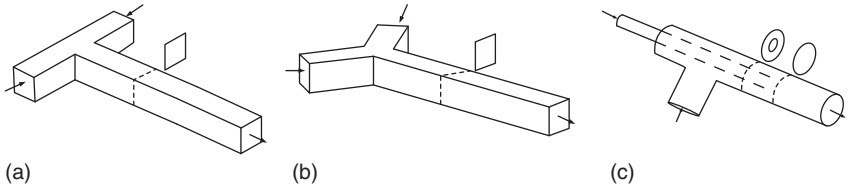

Figure 4.15 Different types of MSR with various contacting geometries and cross sections [27]: (a) T-square, (b) Y-rectangular, (c) concentric. (Adapted with permission from Elsevier.)

The transition of regimes depends on *Re* and reactor geometry. In T-mixer, stratified flow is observed at low *Re*. Engulfment flow is observed at *Re* > about 100. Engler *et al.* [11] proposed a parameter (K) to estimate the flow regime in T-mixers.

$$K = d_h/\lambda_K \tag{4.28}$$

where λ_K is the Kolmogorov length denoting the smallest eddy in a fully developed turbulent flow and is defined as

$$\lambda_K = \left(\frac{\nu^3}{\varepsilon}\right)^{0.25} \tag{4.29}$$

The first transition from stratified to vortex flow was observed at about $K = 15$, whereas the transition to engulfment flow happened at $K = 40$. The corresponding *Re* for two transitions in a $600 \times 300 \times 300$ µm T-mixer are 45 and 150, respectively, which corresponds roughly to the observations presented in Section 4.2**.**

Another way of increasing the mixing efficiency for *Re* in the range of a few hundred is the design of curved channels [28]. Here the mixing quality is improved by creating secondary flow pattern for Dean number (De) > 140, where

$$De = Re\left(\frac{d_h}{R''}\right)^{0.5} \tag{4.30}$$

where R'' is the mean curve radius of the microchannel (see Figure 4.16). The same effect is observed for zig-zag channels, where secondary flow pattern appears at *Re* in the range of a few hundred [29]. In Figure 4.16 the interface stretching factor, λ, is defined as the interface length at a certain position divided by the initial interface length [28]. As can be seen in Figure 4.16, no stretching occurs for $De = 100$, whereas for $De = 200$ the stretching increases exponentially with the number of curved elements in series.

Another type of mixer where both fluids are mixed tangentially or radially (Figure 4.17) are cyclone type mixers that offer high mixing performances [30]. The fluids to be mixed enter the cyclone mixing chamber tangentially via two entry channels creating a swirl motion in the mixing chamber enhancing mixing. The combined fluids exit the cyclone mixing chamber through the exit channel. Mixers with feed channels arranged radially were intended to avoid the swirl motion of the fluids. A similar device was proposed by Arsani *et al.* by using a nonaligned T-mixer [31].

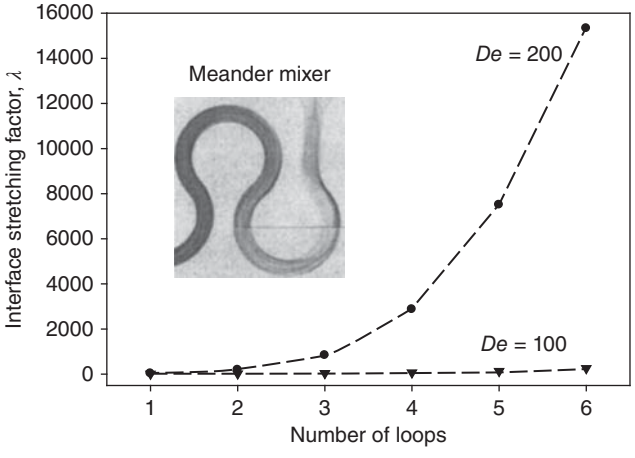

Figure 4.16 Interface stretching factor in meander mixer as function of the number of loops and Dean number [28]. (Adapted with permission from Wiley.)

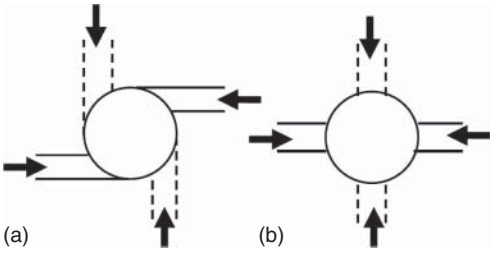

Figure 4.17 Sketch of tangential (a) and radial (b) feed positions for mixers with two and four entry channels [30]. (Adapted with permission from Elsevier.))

4.4.1.2 **Multilamination Mixers**

As we have seen before, stratified flow (two laminations) can be achieved in single-channel micromixers. The benefit of the geometrical focusing can be easily seen by looking at the characteristic mixing time, which in case of a straight rectangular channel with a height, H, comprising two fluid lamellae equals

$$t_{\mathrm{mx}} = t_D = \frac{(H/2)^2}{D_m} \tag{4.31}$$

Thus a reduction of the channel height corresponding to a reduction of the hydraulic channel diameter leads to a decrease of the mixing time. By compressing the fluid lamellae to a few micrometers, the diffusion distances are reduced, corresponding to liquid mixing in the milliseconds range. Similarly, geometric compression, that is, reduction of the flow cross section, can lead to lamellae thinning.

To replicate such a flow in a single device, that is, multilamination, structures with alternate feeds can be created by interdigital (see Figure 4.18a) or bifurcation structures. These lamellae of alternate concentrations decrease the striation

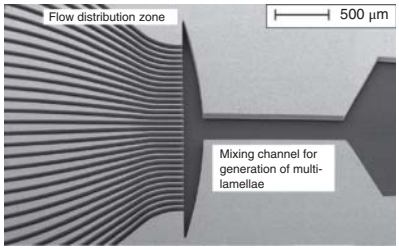

(a) Slit-type interdigital micromixer

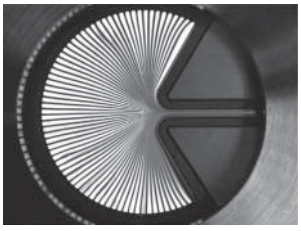

(b) Superfocus micromixer

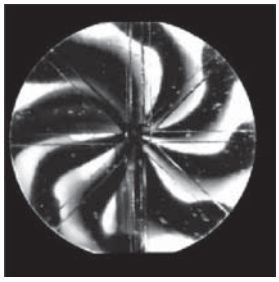

(c) Flow pattern in a cyclone micromixer

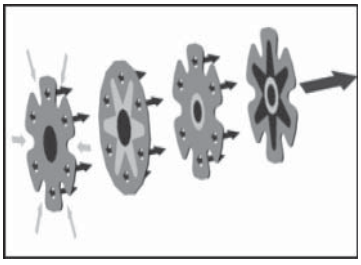

(d) Star lamination micromixer

Figure 4.18 Different types of multilamination micromixers. (a) liquid flows 10–1000 ml h^{-1}, (b) 138 microchannels flow: 350 l h^{-1} at 3.5 bar, (c) 20 ml h^{-1}, and (d) snapshot of mixer for throughput <300 l h^{-1}, pressure drop 7.6 bar [32]. (Adapted with permission from Elsevier.)

thickness resulting in low diffusion time. Multilaminating flow configurations can be realized by different types of feed arrangements. Bifurcation-type feeds create an alternate arrangement of feeds. Such a laminated feed stream passes into an inverse bifurcation structure and a subsequent folded delay-loop channel where mixing takes place. The channel width of the feeds of most interdigital arrangements is chosen in a way that the width of the corresponding liquid lamellae is rather thick (e.g., 100 µm), that is, diffusion is not very effective. Therefore, a second momentum for speeding up mixing is employed. In analogy to the well-known hydrodynamic focusing concept (for a single stream or for two streams), the multilaminated flows are focused by posing geometric constraints (typically a triangular focusing chamber), thereby compressing the lamellae.

The flow patterns in liquids can be confirmed using photographic analysis before and after focusing. These lamellae can tilt and, at high *Re*, spirally wind and form recirculations, if the focusing angle is set too large. In the case of gas mixing in an interdigital microstructured mixer, similar periodic multilamination patterns were determined by a tiny gas-collecting nozzle that was moved within the mixing chamber of interdigital mixers. At high velocities of the gas streams, anomalously high mixing efficiencies were found at a certain axial distance along the mixing chamber. This observed faster mixing was explained with additional turbulent mixing because of the collision of gas streams owing to the tilted injection via

the interdigital feed. It was found that the mixing energy of these microstructured mixers normalized by the volume for a given mixing task is lower than that of an industrially employed jet mixer.

A special liquid focusing interdigital mixer with parallel feed flows, termed *SuperFocus*, was optimized by semianalytical calculations and first realized as a glass version with 128 nozzles ($8\,h^{-1}$ at 3.5 bar) and later as a steel version ($350\,h^{-1}$ at 10 bar) with 138 nozzles. Both versions yield 4 µm thin liquid lamellae. A mixing time (for 95% completion of mixing) of 4 ms, excluding the time needed for passing the focusing chamber, can be obtained by photometric measurement for the SuperFocus mixer, corresponding to some centimeter mixing length at most practical throughputs. Different cross sections are used to optimize the focusing chamber to reduce the residence time within this flow passage to shorten the overall mixing time.

The cyclone mixer is another micromixer that can also be multilaminated. In the high-throughput Star laminators (Figure 4.18d), the fluid feed resembles an alternating (interdigital) flow injection. Owing to the large internal opening and the typically applied large volume flows, the flow regime, however, is turbulent so that a prelayered flow is consecutively mixed by eddy formation. As the plates can be manufactured at low cost and a large number of plates, for example, several hundred, can be stacked, extremely large throughputs can be achieved already for devices of small external volume (*StarLam300* – $1000\,l\,h^{-1}$ (3 bar) and *StarLam3000* – $5\,m^3\,h^{-1}$ (about 3 bar)). The determined mixing efficiencies reach the limits that are usually attributed to good mixing in macro- and microstructured mixers.

4.4.1.3 Split-and-Recombine (SAR) Flow Configurations

Unlike commonly applied interdigital multilamination approach, split-and-recombine (SAR) mixing relies on a *multi*step procedure. According to its name, the basic operations are the splitting of a bi- or multilayered stream perpendicular to the lamella orientation into substreams and their subsequent recombination [33]. This concept is schematically represented in Figure 4.19a. For this purpose, basically three steps are required: flow splitting, flow recombination, and flow

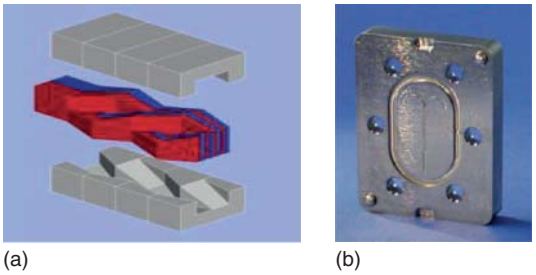

(a) (b)

Figure 4.19 Caterpillar mixer. (a) Schematic of SAR showing structured walls. (b) Snapshot of the 600 µm size caterpillar mixer. The size is defined for entrance channel. Courtesy Fraunhofer ICT-IMM, Germany.

rearrangement. The flow splitting in SAR mixers is superimposed by secondary recirculation flow patterns at most practical *Re* and for most liquids. It was further noted that SAR flows, although ideally highly regular, have features of chaotic mixing, as they benefit from an exponential increase in interface similarly to the chaotic stretching.

This flow configuration has been used in the so-called caterpillar micromixer (Figure 4.19b) that is commercially available. This micromixer exists in different configurations with standard mixing size ranging from 150 to 2400 μm and a flow rate up to 250 l h^{-1}.

The micromixer with structured internal surfaces (e.g., caterpillar mixer, discussed in the later section) show different trends compared to the other microchannels. It shows quadratic dependency of the pressure loss on the flow velocity according to the following equation [16]:

$$\Delta P = \zeta_{\text{total}} \frac{\rho}{2} u^2 = \left(\zeta_{\text{vortex}} + \frac{\zeta_{\text{friction}}}{Re} \frac{1}{d_h} \right) \frac{\rho}{2} u^2 \tag{4.32}$$

where, ζ_{friction} is the constant multiplication factor originating from wall friction and ζ_{vortex} is the multiplication factor originating from both flow bending and vortex creation. The quadratic dependency originates from the laminar operation of the mixing devices combined with induced vortices in the mixing elements.

4.4.1.4 Mixers with Structured Internals

The mixers with structured internals differ from SAR because of the fact that in the latter case the walls are structured to create chaotic mixing. In this case, the mixers have internal 3D structures, like structured packing, for distributive mixing as for conventional static mixers. Static mixers divide and conquer the flow, where the liquid to be mixed is divided into smaller streams. These streams are interwoven in such a way as to reduce the distance that molecules need to diffuse and, therefore, to reduce the mixing time. Microstatic mixers are fabricated using stereo lithography technique (Figure 4.20). Besides having additional structures within the whole channel, they may be placed only on one channel side, yet altering the profile in the complete flow domain. The intersecting device provides manifold splitting and recombining of the flow, yielding a fine-dispersed system compared to the helical device. Generally, the mixing performance and periodicity of the functional elements can be correlated and the shortest mixing length can be achieved using more functional elements [34].

4.4.1.5 Chaotic Mixing

The chaotic mixing is characterized by an exponential rate of stretching, as opposed to linear stretching in nonchaotic flow of fluid elements [17] resulting in exponential growth of the interfacial area accompanied by a corresponding reduction of the striation thickness. Chaotic advection can occur either by two-dimensional unsteady velocity fields or by three-dimensional velocity fields with or without time dependence. Many of the active mixing principles fall into the former class. The chaotic advection can be generated by placing microstructured

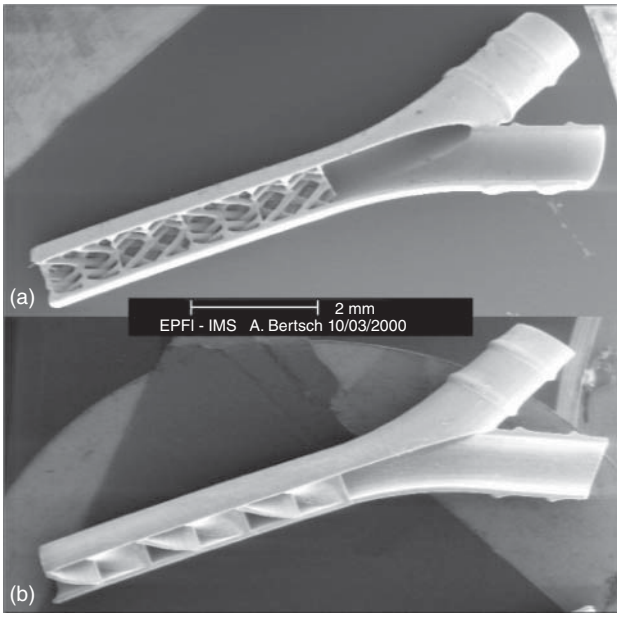

Figure 4.20 Structured packing for flow configurations: the intersecting device (a) and helical device (b) [35]. (Reproduced with permission from The Royal Society of Chemistry.)

objects within the flow passage on one or two sides of the microchannels. By this means, flow circulations are generated, which lead to an exponential increase of specific interface, hence to fast mixing. Typical for such chaotic flows are circulating fluids with large interfaces besides quiescent zones with less improved mixing. One of the pioneering descriptions presents a staggered herringbone mixer (SHM) [36, 37].

High-resolved cross-sectional images of the flow were presented, showing the ongoing folding of the initial lamellae after passing the cycles defined by the herringbone pattern. The mixing efficiency can be further increased by using belayed SHM [38]. The particularity of herringbone micromixers is their high performance at very low *Re* (<10). This is in contrast to most of the conventional chaotic mixers (Figure 4.21).

4.4.1.6 Colliding Jet Configurations

Handling of solutions, which produce particles in the abovementioned micromixers is challenging as it may block the channel, which results in a risk in the operation. In this case, jet mixing technology is used which vary from low [39] to high velocity turbulence jets [40]. A complete system with jet collision at very high velocities is commercially available and versatile in application, that can be used for powder synthesis and emulsification. A low-velocity jet collision device with Y-type flow configuration, with free guided jets, has been realized for conducting reactions that lead to immediate and heavy precipitation (see Figure 4.22) [39].

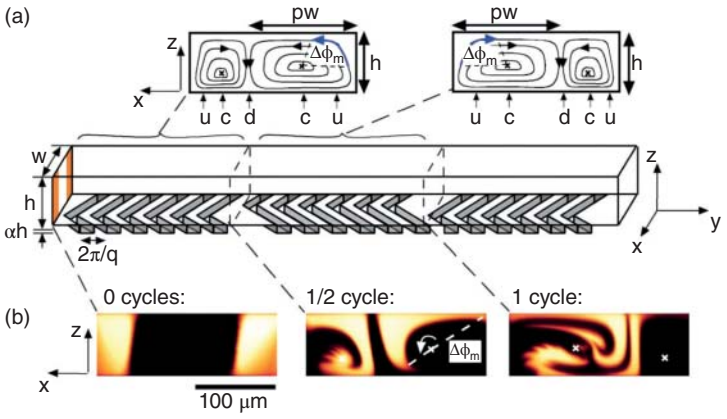

Figure 4.21 Staggered herringbone mixer (SHM). (a) Schematic diagram of one-and-a-halfcycles of the SHM. (b) Confocal micrographs of vertical cross sections of a channel. $h = 77$ μm, $w = 200$ μm, $\alpha = 0.23$, $pw = 2/3w$, angle of the ridges with respect to the channel, $\theta = 45°$, $Re < 0.01$ [36]. (Adapted with permission of The American Association for the Advancement of Science.)

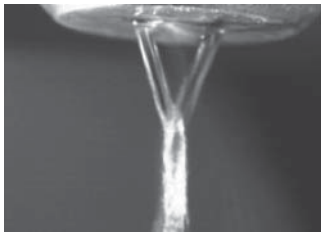

Figure 4.22 Y-type jet generated by a jet micromixer. (Adapted from Ref. [39] (Courtesy Fraunhofer ICT-IMM, Germany.)

This system was successfully applied to the quaternization of ternary amines and the base-assisted amide formation, both of which are known not to be feasible in other standard microchannel devices.

4.4.1.7 **Moving Droplet Mixers**

In the case of laminar flow in a straight channel, the parabolic velocity profile is observed as shown in Figure 4.23a, which leads to the broad residence time distribution in the reactor, and thus the performance of the reactor deviates from that of ideal plug flow [41] (see also Chapter 3). Conventionally, the turbulent flow is used to avoid the axial dispersion. In micromixer, the plug flow profile can be achieved by binding the reaction partners in the form of slugs (or plugs) that give every molecule the same processing experience as shown in Figure 4.23b. It offers rapid mixing by internal circulation with negligible residence time distribution, making it suitable for controlling reaction and mixing operations.

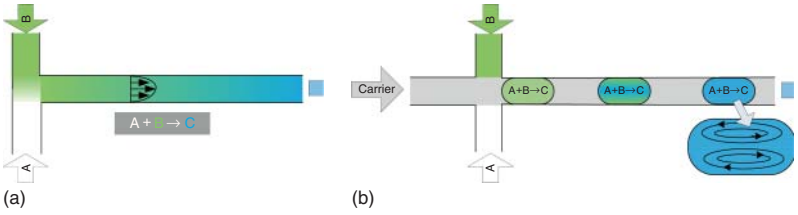

Figure 4.23 Moving droplet mixers (schematic): (a) typical laminar profile, (b) homogeneous mixing in biphasic mode.

Different arrangements, axial and radial arrangements of reactants within slugs, can be achieved with the former arrangement of reactants giving higher mixing performances than the radial arrangement at the same Peclet number [42]. Besides, bending the microchannels in different angles mixing in the slugs can be altered as shown in Figure 4.24.

This concept is also used for kinetics study of fast homogenous reactions with characteristic reaction times in the range of milliseconds. Further examples are precipitations and the reactions that use reagents in the nanoliter scale.

Another method of droplet-based mixing is via electrowetting, which is based on the change of surface energies by applying electric fields [44]. This technique differs from continuous flow systems in which discrete droplets are manipulated rather than continuous liquid streams and possess a number of advantages over the latter such as the ability to control each droplet independently, enabling

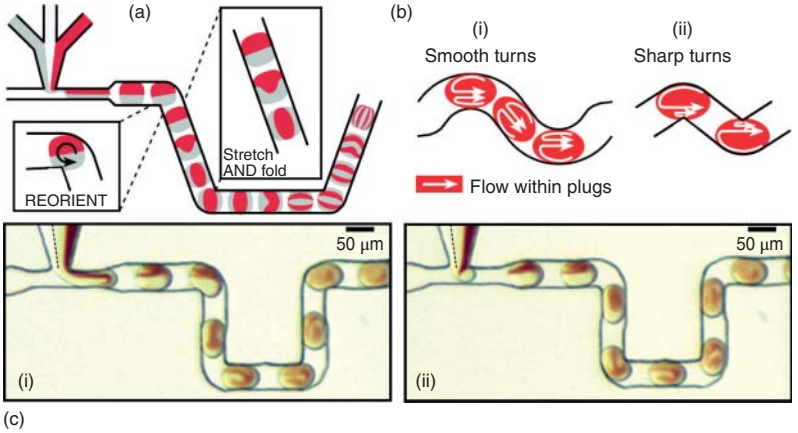

Figure 4.24 Chaotic mixing in droplets [43]. (a) Schematic of straight portions of the channel performs stretching and folding, and turns allow for reorientation. (b) Schematic of recirculating flow in plugs moving through smooth and sharp turns. (c) Snapshots of the microfluidic network in which flow patterns inside plugs in different positions in the microchannel demonstrate flow patterns. (Adapted with permission from The Royal Society.)

complex procedures to be performed in a manner similar to traditional batch-type protocols. There are many combinations of moving, splitting, and merging droplets. Reconfigurable flow and the absence of permanently etched channels also allows for a highly integrated, scalable, and flexible architecture. The size of the droplet is chosen so that it is slightly larger than the area of one electrode segment, that is, partly overlaps with the adjacent electrodes. For example, the electrode gap was set to 800 µm, the droplet volume was 1.9 µl, and a voltage of 50 V was applied [44]. If mixing is achieved by droplet movement only, this is passive mixing owing to convections. If the droplets can be shaken, then it is an active mixing (described in the later part). The passive mixing does not lead to effective mixing, rather a vertically layered structure within the droplet is produced that mixes only via diffusion requiring a long time of 1 – 2 min.

4.4.1.8 Miscellaneous Flow Configurations

There are several miscellaneous passive mixers that have been used for case-specific applications by modifying the abovementioned principles. Some of them are presented here.

One of the passive mixers was developed using capillary forces to insert and hold the liquids in separate chambers, which are connected via a small gap [45]. It is a self-filling micromixer device and does not require micropumps referring it as an automixing device. This device was developed on a chip with two channels with variable volumes that are separated by a thick porous plate through which mixing takes place by diffusion. The idea was to use the capillary forces to fill one capillary with two liquids.

One of the promising designs is the modified Tesla structures [46]. It uses the Coanda effect to split part of the fluid stream and direct it so that it recombines with the opposing flow of the other part of the stream. Coanda effect micromixer relies on the redirection of a flow by a special guiding structure that creates new interfaces within the flow [47]. This special passive structure provides good mixing at low flow rates. In this way the Coanda mixer can also be seen as a special realization of the SAR approach using recycle flows [32].

Another passive mixer termed as a *microfluidic baker's transformation* (*MBT*) device was developed for rapid mixing in a microchannel [48]. It has successive 3D configuration changes to realize folding, stretching, cutting and fusing of microfluids. The mixing mechanism was based on the baker's transformation, an ideal mixing method, as a chaotic mixer and complete mixing was achieved in a few hundred ms residence time in 10.4 mm mixing length microchannel. The Peclet number as high as 6.9×10^4 was obtained.

An integrated mixer/valve with a cantilever-plate flapper valve allows for non-continuous mixing by diffusion [49]. The mixer/valve consists of two wafers: (i) a lower silicon wafer with a cantilever-plate flapper valve and fluid ports and (ii) an upper glass wafer that contains the fluidic channel. Initially the sample flows down the channel. When it is time to mix a reagent with the sample, the reagent is injected into the sample stream, and the two mix diffusively in a few seconds. After the desired section of sample is prepared, the reagent is shut off and the mixed

sample and reagent flow down the channel and out of the mixer/valve. The liquid mixer/valve is controlled by varying the reagent and sample flow rates. The relative flow rates in turn determine the mixing ratio and the pressures at the reagent and sample ports; the cantilever plate aligns itself accordingly.

4.4.2 Active Micromixers

In contrast to the presented passive mixers, active micromixers rely on external power input to introduce perturbations within the laminar flow to accelerate mixing. A selection of different external perturbation sources are summarized in Table 4.1 and are discussed briefed here.

4.4.2.1 Pressure Induced Disturbances

Mixing in stratified laminar flow relies on molecular diffusion. Therefore, mixing time for liquids is in the order of seconds in microchannels with diameters in the range of about 100 µm. A very simple method to disturb the fluid flow consists in superimposing a pulsating flow in the inlet of the channels. Glasgow and Aubry [50] used a simple T-shaped mixer to demonstrate the effective flow disturbance at very low *Re* ($\geq$0.3) by varying the inlet flow in a sine wave fashion.

Time pulsing of one inlet flow rate distorts the interface to an asymmetrically curved shape, which changes with time-influencing material transport and thus the mixing. The periodicity and the number of pulsing streams have a notable influence of the mixing efficiency. The best results are reported for two pulsed inlet flows having a phase difference of 180° with amplitude and frequency being the same [50]. The simulated results are reproduced in Figure 4.25 for a mean flow velocity of 1 mm s^{-1} and a perturbation frequency of 5 Hz. Besides, the bending of the fluid interface along the channel cross section and the respective stretching and folding in the direction of the flow increases the mixing further. This concept can be extended to the multiple, pulsing injection of flows into one microchannel; such devices are so far hypothetical and certainly would require a complex control system [51]. By these means, chaotic advection can be generated.

For electroosmotic-driven flow, periodic flow switching can be achieved in a similar way, now by using nonuniform ξ potentials along the conduits walls to induce chaotic advection [52]. Both spatial and temporal control of the ξ potential can be achieved by imposing an electric field perpendicular to the solid–liquid interface. The nonuniformity of the ξ potentials induces complex flow patterns in the conduit. By appropriate time modulation of the ξ potential, one can alternate among two or more flow patterns and induce chaotic advection and efficient stirring in the conduit. There are many choices for possible flow patterns. The selection of combinations that lead to the most efficient stirring process is an interesting optimization problem. Such a method is particularly beneficial for microfluidic systems where incorporation of moving components is difficult.

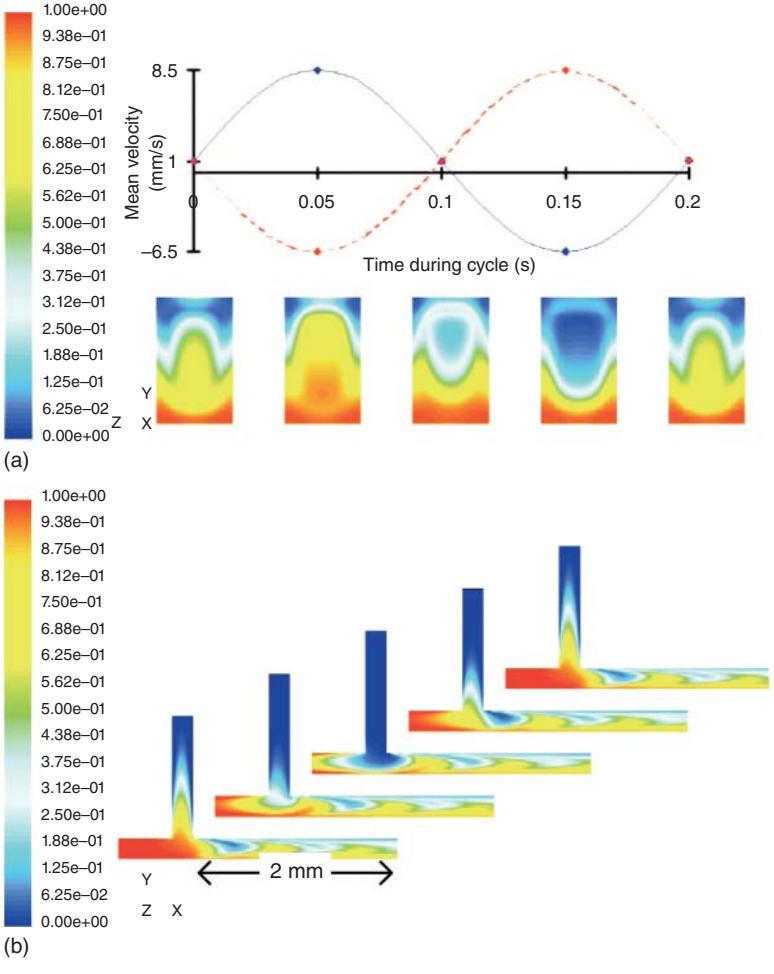

Figure 4.25 Simulated results for periodic pressure field disturbance [50]: (a) mean liquid velocity as function of time for the in-line inlet (dashed line) and the perpendicular inlet (solid line). Contour levels of the mass fraction of the fluids in the Y–Z plane. (b) Contour levels in the Y–X plane as function of time as shown in (a). (Adapted with permission from The Royal Society of Chemistry.)

4.4.2.2 Elektrokinetic Instability

Mixing can be achieved by initiating a flow instability, which are observed in sinusoidally oscillating, electroosmotic channel flows referred to here as *electrokinetic instability* (*EKI*) [53]. In this way, rapid stretching and folding of material lines are induced, similar to the effect of stirring accomplished by the action of fluctuating electric fields [53]. Most common, sinusoidal oscillation of electric fields is applied. EKI is adequate for mixing flows at very low *Re* (~1). In one realized example, comparatively low frequencies, below ~100 Hz, and electric field strengths in excess of 100 V mm^{-1} were applied for channels with dimensions of

about 50 µm. A small square mixing chamber is connected to two opposite electrodes; the two liquids are fed in 90° orientation to the electrodes into the chamber and one outlet is placed on the side of the chamber (see Figure 4.26).

4.4.2.3 Electrowetting-Induced Droplet Shaking

Droplets can be actuated through electrowetting in which the interfacial tension of the droplets is modulated with voltage [44]. In this case, the merged droplets are shaken using multielectrode arrays resulting in an effective mixing compared to passive mixing of merged droplets. The volume of the droplet is chosen to ensure an overlap between the droplet and adjacent electrodes. A typical example is using a four-electrode array (600 µm electrode gap; 8 Hz, 1.32 µl droplet volume; 50 V) that creates complex patterns of fluid giving much reduced mixing times [44].

4.4.2.4 Ultrasound/Piezoelectric Membrane Action

Ultrasound vibrations are shown to be effective in many applications to improve mixing processes. The liquid streams can be moved and even turbulent-like eddies can be induced. In such micromixer, mixing can be achieved by ultrasound using lead–zirconate–titanate (PZT) membranes, a piezoelectric ceramic, operated in the kHz range [54] or a thin piezoelectrically actuated membrane [55]. In the latter case, the impact of the frequency and amplitude of actuation on the mixing efficiency shows that an optimum signal amplitude between 30 and 40 V was found corresponding to a total membrane stroke of 6.7 µm. For lower voltages, mixing

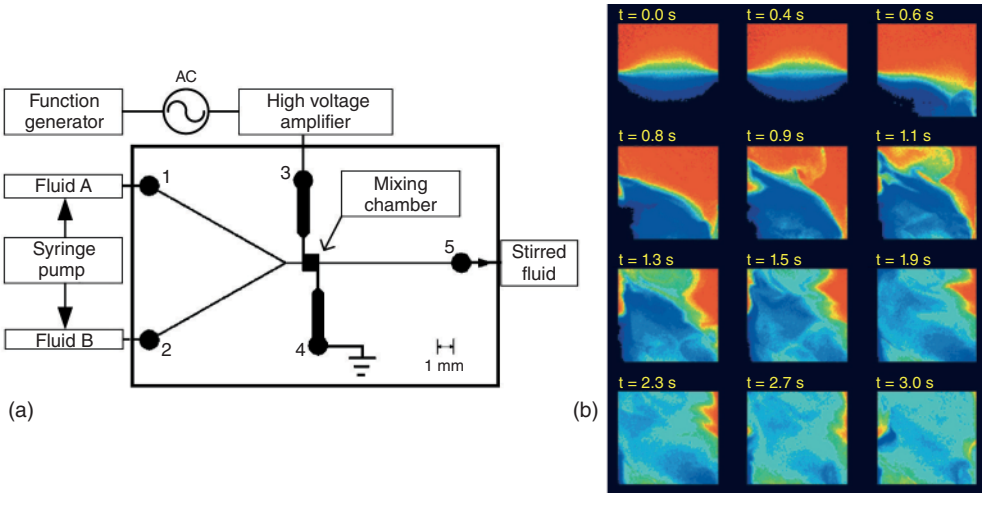

Figure 4.26 Design of an electrokinetic instability micromixer. (a) The electrokinetic instability is confined to the square mixing chamber shown in the center of the schematic and, to a small part, to fluid channel regions attached to it. (b) Complex fluid motion generated in the mixing chamber. (Adapted with permission from Ref. [53]. Copyright (2001) American Chemical Society.)

is incomplete. At higher amplitude, no further improvement was noted. Owing to the very small mixing chamber, fast changes of mixing can be induced.

4.4.2.5 **Acoustic Fluid Shaking**

An air bubble in a liquid medium can act as actuator (i.e., the bubble surface behaves like a vibrating membrane), when the bubble undergoes vibration within a sound field [56]. The behavior of bubbles in sound fields is determined largely by their resonance characteristics (Figure 4.27).

Such a mixer consists of a piezoelectric disk (PZT) that is attached to a reaction chamber designed in a way that a set of air bubbles with desirable size is trapped in the solution. Bubble vibration because of a sound field induces friction forces at the air/liquid interface, which causes a bulk fluid flow around the air bubble, termed *cavitation microstreaming* or *acoustic microstreaming*. The bubble-induced streaming is strongly dependent on frequency for a given bubble radius. Acoustic microstreaming arising around a single bubble excited close to resonance produces strong liquid circulation flow in the liquid chamber. This liquid circulation flow can be used to effectively enhance mixing.

Sonic irradiation without the use of air bubbles causes only little fluid motion and, therefore, bubbles are used [57]. Because of the uniform distribution of the air pockets, mixing is induced in the complete microchamber and not localized to one part only. The mixing time can be improved by increasing the number of bubbles. For example, in a dilution-type experiment, the mixing time using one bubble in a drum-shaped microchamber (300 µm depth; 15 mm diameter) was 110 s, which was reduced to 45 s using four bubbles [56] – an improvement in the mixing time of about 60%.

4.4.2.6 **Microstirrers**

The stirred tank reactor is one of the most commonly used equipments in chemical engineering. In micromixers, such micromagnetic rotating bar stirrers and

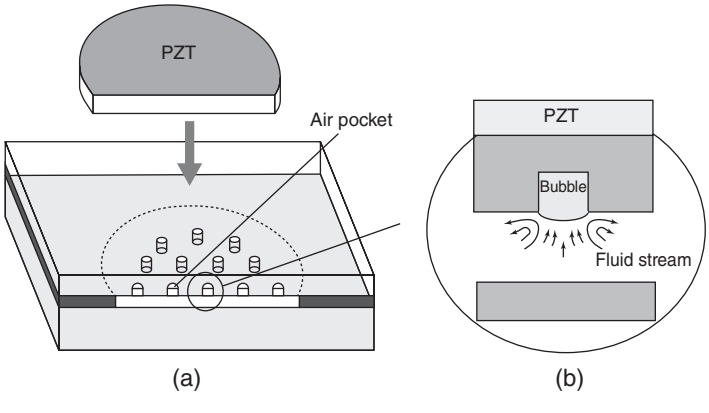

Figure 4.27 Schematic showing air pockets on the inner wall of the mixing chamber. (a) Overview; (b) side view. (Adapted from Ref. [56]. With permission of The Royal Society of Chemistry.)

arrays have been designed using the principles of macroscopic mixers [58]. The centerpiece of the mixer is a rotating bar (rotor) made of a ferromagnetic material consisting of a cap, hub, and two rotary blades. The new mixing principle offers several advantages like rapid mixing that can be realized within the characteristic length of a stirrer bar and externally applied magnetic actuation, which requires no wires and reduces complexity.

The mixer can be used for a wide variety of fluids with different electrochemical characteristics.

4.4.2.7 Miscellaneous Active Micromixers

A special micromixer has been designed for cyclic reaction using alternating current (AC) magnetohydrodynamic (MHD) actuation [59]. It utilizes arrays of electrodes deposited on the walls of a microchannel. The experimental apparatus comprised an AC power source connected in series to the MHD chip and an electromagnet. Through alternate potential differences across pairs of electrodes, currents in various directions of the mixing volume are generated. By coupling an electric and a magnetic field, forces are exerted on the fluid. The MHD actuation is favored for applications involving strong electrolytes or even ionic liquids, where pumping methods such as electroosmotic flow are compromised. Annular MHD reactors are one of the examples of systems for conducting architecture-controlled chemistry, meaning the chemistry that requires careful consideration of channel design, material choice, and actuation technique.

4.5 Experimental Characterization of Mixing Efficiency

For the proper design of a chemical reactor, the mixing time for the separated fed reactants must be adapted to the reaction kinetics and the characteristic reaction time (see Section 4.1). A variety of different experimental methods are developed and used to characterize the mixing process. These methods can be broadly classified as physical and chemical methods. The application of these methods depends on the size of mixer, optical characteristics of the wall material, that is, transparent or opaque, flow throughput, and the precision of mixing quality needed for a given application of mixer. The mixing quality is defined either in terms of degree of segregation (no mixing) or intensity of mixing.

Danckwerts defined the intensity of segregation in turbulent flow, I_s, in terms of the mean square of the concentration fluctuation as shown in Figure 4.3 and defined in Equations 4.1 – 4.4. The efficiency of mixing is in the range between 1 and 0.

4.5.1 Physical Methods

Physical methods to characterize the mixing efficiency are based on the use of an inert tracer, which differs in color, conductivity, or optical density from the main

fluid. The tracer concentration is monitored by measuring the color, electrical conductivity, pH, and so on as function of time. One of the prerequisites for the use of optical method is that the micromixer should be transparent to track the color change of mixed solutions with a reasonable spatial resolution. Visualization of the color spreading along the channel of a continuous mixer using a high-resolution photographic system gives information about the mixing process.

In a more precise method of investigation, the local concentration in a controlled volume is considered. This allows determining the concentration fluctuations referred to the mean.

It is evident that the degree of mixing measured experimentally will depend on the spatial resolution of the probe used to estimate the local concentration in the mixture. Depending on the kind of application, a decrease in the length scales on which these variations are present or reduction in their amplitude or both are desired.

There are several limitations to optical techniques as described in the following:

- The visualization is done usually perpendicularly to the flow direction, and therefore, the analyzed image gives color intensity value over a mixer depth meaning that the visually uniform color concentration may be interpreted either as a complete mixing or as a regular multilamellae flow of various concentrations. This results in inappropriate investigation of mixing time.
- Besides, even in the case of transparent device, the analysis can be done only for very simple microchannel geometry without internal structures.
- Finally, if the sampling volume is larger than the smallest segregation scale, then it is difficult to determine whether the two fluids are mixed or not within the measurement resolution.

4.5.2 Chemical Methods

As explained before, physical methods possess severe limitations and, therefore, chemical methods have been developed to characterize the mixing efficiency. In this case, very fast reactions that are strongly influenced by mixing are used and the amount of product formed represents the mixing quality in the mixer. However, if a single reaction is used, it requires the online measurement of local species concentration along the flow. With such systems, one experiences the main drawback of physical methods with the difficulty of local measurement and the influence of the probe size on the mixing quality estimation. Therefore, offline measurement is warranted. These methods are described in the following.

4.5.2.1 Competitive Chemical Reactions

The principle of competitive chemical reactions is based on the fact that when the characteristic mixing time and characteristic reaction time are of the same order of magnitude, two processes will compete resulting in lower consumption rate of

reactants than the intrinsic reaction rate. Using the models that couple mixing and reaction kinetics, the mixing time can be estimated.

Two types of competitive reactions, consecutive and parallel, have been proposed to investigate the mixing process efficiency:

$$\begin{aligned}&\text{Consecutive competitive reactions}:\\&\text{(a)}\,A_1 + A_2 \rightarrow A_3\\&\text{(b)}\,A_3 + A_2 \rightarrow A_5\end{aligned} \tag{4.33}$$

$$\begin{aligned}&\text{Parallel competitive reactions}:\\&\text{(a)}\ A_1 + A_2 \rightarrow A_3\\&\text{(b)}\ A_4 + A_2 \rightarrow A_5\end{aligned} \tag{4.34}$$

In both cases the first reaction (Equations 4.33a and 4.34a) is instantaneous (e.g., a neutralization) while the second reaction has characteristic reaction time comparable to the characteristic mixing time. The reactant A_2 is added in an overall stoichiometric defect to the stream of A_1 in consecutive reactions or to the stream of solution containing A_1 and A_4 in parallel reactions. If the aggregates of A_2 are rapidly mixed forming homogenous solution with a rate much faster than the rate of the second reaction ($t_{\mathrm{mx}} \ll t_{r,\,b}$), species A_2 will be almost totally consumed by the first reaction and no A_5 will be formed. However, if mixing is slow, local over-concentration of A_2 as compared to A_1 will develop and A_5 will be formed. Thus, the concentration of A_5 is a measure for the mixing rate in the device – the higher the concentration of A_5, the slower the mixing process and vice versa. The A_5 concentration is measured at the reactor outlet and the global mixing parameter along the reactor is obtained. The limitation of this method is that it does not indicate the mixing efficiency in the confined zone within the mixer where it is needed.

Some of the chemical methods that have been used to investigate the mixing quality in different types of reactors are briefed in the text below. Most of the methods were developed for batch wise operated reactors and must be revisited and carefully adapted for the use in continuous microstructured devices.

Neutralization and Ester Hydrolysis This set of competitive reactions consists of adding a NaOH solution to a more dilute solution of HCl and ethyl monochloroacetate [60].

$$\begin{aligned}&\mathrm{NaOH} + \mathrm{HCl} \xrightarrow{k_1} \mathrm{NaCl} + \mathrm{H_2O}\\&\mathrm{NaOH} + \mathrm{CH_2ClCOOC_2H_5} \xrightarrow{k_2} \mathrm{CH_2ClCOONa} + \mathrm{C_2H_5OH}\end{aligned} \tag{4.35}$$

These test reactions exhibit several suitable features, for example, known kinetics, partial segregation at molecular scale, a product distribution characterizing the degree of micromixing, simple chemical analysis, and many degrees of freedom for the experimentalist. During the experiments, the product distribution is determined by GC analysis of either the residual ester or of the ethanol formed.

Further hydrolysis of the acidic sample before GC analysis is almost negligible as the non-catalyzed hydrolysis is very slow.

When studying the influence of micromixing on the product distribution of three parallel reactions, the alkaline hydrolysis of methyl chloroacetate is employed as the third reaction supplementing the existing ones:

$$NaOH + CH_2ClCOOCH_3 \xrightarrow{k_2} CH_2ClCOONa + CH_3OH \tag{4.36}$$

The alkaline hydrolysis of the methyl ester (Equation 4.36) is faster than that of the ethyl ester (Equation 4.35).

Diazo Coupling The diazo coupling between 1-naphthol and diazotized sulfanilic acid is a competitive-consecutive reaction that gives two primary couplings to produce isomeric mono-azo dyes (*para* and *ortho*) and their secondary coupling to give finally one bisazo dye [61]. The product distribution between mono- and bisazo dyes is sensitive to mixing and can be used to determine the rate of mixing in the reaction zone.

The reaction is exothermic ($\Delta H_r = -100\,\mathrm{kJ\,mol^{-1}}$) and the activation energy is $39\,\mathrm{kJ\,mol^{-1}}$. Therefore, lower concentrations are used to minimize the temperature rise. The product distribution, after the limiting reagent (diazotized sulfanilic acid) has been fully consumed, is considered to characterize the mixing quality.

Competitive Neutralization and Acetal Hydrolysis In this method, HCl is fed to a mixture of NaOH and 2,2-dimethoxypropane (DMP) and the following reactions take place [62, 63]:

$$HCl + NaOH \xrightarrow{k_1} NaCl + H_2O$$

$$H_3CC(OCH_3)_2CH_3 + H_2O \xrightarrow[H^+]{k_2} (CH_3)_2CO + 2CH_3OH \tag{4.37}$$

The first reaction (neutralization) is nearly instantaneous ($k_1 = 1.4 \cdot 10^8\,\mathrm{m^3\,(mol\,s)^{-1}}$ at 298 K) relative to mixing, irrespective of temperature and reagent concentrations. It is irreversible and moderately exothermic ($\Delta H_r = -55.8\,\mathrm{kJ\,mol^{-1}}$). The second reaction is irreversible in diluted aqueous solution and catalyzed by acids. When the characteristic mixing time is short relative to the characteristic reaction time of the slower reaction, the system reaches a homogenous condition. As the first reaction is much faster than that of the DMP hydrolysis, HCl will be consumed too quickly for DMP to react and, therefore, acetone or methanol will not be generated in detectable quantities. However, when the characteristic mixing time is longer or equal to the characteristic reaction time of the slower reaction, a local concentration gradient exists at the fluids interface, where NaOH will react immediately with HCl creating a NaOH depleted zone. The interface becomes rich with DMP, allowing it to hydrolyze with HCl. Thus, the yield of methanol gives the quality of mixing.

This reaction has been tested with a minimum concentration of $0.1\,\mathrm{mol\,l^{-1}}$ of NaCl to ensure consistent kinetics of the neutralization and hydrolysis reactions [63].

Villermaux-Dushman Reaction This method, also referred to as *iodide-iodate reaction*, is based on a system of two parallel competing reactions [64]:

$$\begin{aligned} H_2BO_3^- + H^+ &\xrightarrow{k_1} H_3BO_3 \qquad r_1 - \text{instantaneous reaction} \\ 5I^- + IO_3^- + 6H^+ &\rightleftharpoons 3I_2 + 3H_2O \qquad r_2 - \text{fast reversible reaction} \end{aligned} \tag{4.38}$$

The first reaction is a neutralization, which can be considered as instantaneous, while the second one is fast. The reaction rate, r_2, depends on the concentration of the reaction partners and can be described with the following kinetic model [65]:

$$r_2 = k_2 \cdot c_{H^+}^2 \cdot c_{I^-}^2 \cdot c_{IO_3^-} \tag{4.39}$$

where the rate constant k_2 is a function of the ionic strength of the solution.

To characterize the mixing in microstructured devices, two solutions – a buffer solution of $H_2BO_3^-$, I^-, and IO_3^- and a diluted sulfuric acid solution – are fed to the mixer. In the case of ideal mixing, the acid is instantaneously distributed homogenously and is completely consumed by the borate ions to form boric acid; in consequence, the second reaction will not take place. However, if immediate mixing is not achieved, acid aggregates will persist for some time and the iodide-iodate reaction takes place leading to the formation of iodine. Hence, the selectivity to iodine characterizes the mixing performance: the lower the concentration of iodine formed, the faster the mixing is achieved.

There is a prerequisite of pH for both the reactions to occur. If the pH value of the mixture is low, iodine is continuously formed although mixing is already complete. Therefore, the overall final pH in the mixer should be close to 7 in order to confirm that the formation of iodine is only because of imperfect mixing in the microchannel [64]. The iodine formed reacts further with iodide ions (I^-) to form I_3^- ions, which can be detected by UV-VIS spectroscopy.

$$I_2 + I^- \rightleftharpoons I_3^-; K_C = \frac{c_{I_3^-}}{c_{I_2} \cdot c_{I^-}} \tag{4.40}$$

The equilibrium constant K_C is a function of temperature (T) and can be calculated with the following relation:

$$\log_{10} K_C = \frac{555}{T} + 7.355 - 2.575 \cdot \log_{10} T \tag{4.41}$$

The absorbance (A) of I_3^- is measured and the concentration is obtained from Beer-Lambert law [64]:

$$c_{I_3^-} = \frac{A}{\varepsilon_{353} \cdot l}; \varepsilon_{353} = 2606\,\text{m}^2\,\text{mol}^{-1} \tag{4.42}$$

where ε_{353} is the molar extinction coefficient at a wave length of 353 nm and l is the optical path length of the spectroscopic cell. The acid concentration of the reaction needs to be chosen properly so that the amount of iodine formed should be in the range of acceptable UV absorbance. The Beer-Lambert law used to determine the concentration from absorbance (A) is valid for absorbance in the range of $0.1 < A < 2.5$.

The mass balance for the iodine atoms yields the following expression [64]:

$$c_{I^-} = c_{I^-,0} - \frac{5}{3} \cdot (c_{I_2} + c_{I_3^-}) - c_{I_3^-} \tag{4.43}$$

With the known equilibrium constant, the iodine concentration can be determined:

$$-\frac{5}{3} \cdot c_{I_2}^2 + \left(c_{I^-,0} - \frac{8}{3} \cdot c_{I_3^-}\right) \cdot c_{I_2} - \frac{c_{I_3^-}}{K_C} = 0 \tag{4.44}$$

The mixing quality can be expressed in terms of a segregation index (X_S) defined in Equation 4.45, which lies between 0 and 1. $X_S = 1$ corresponds to complete segregation and the segregation $X_S = 0$ is obtained for ideal molecular mixing.

$$X_S = \frac{Y}{Y_{CS}} \tag{4.45}$$

where Y denotes the ratio of the quantity of acid moles consumed by the second reaction (Equation 4.38) and the total amount of acid fed to the system. Y_{cs} is the value for complete segregation. For a continuous mixer with equal flow rates of both solutions, the equations for Y and Y_{CS} can be written as

$$Y = \frac{4 \cdot (c_{I_2} + c_{I_3^-})}{c_{H^+,0}} \tag{4.46}$$

$$Y_{CS} = \frac{6 \cdot c_{IO_3^-,0}}{6 \cdot c_{IO_3^-,0} + c_{H_2BO_3^-,0}} \tag{4.47}$$

where subscript 0 denotes the inlet concentrations of the component in the respective solutions. The use of the Villermaux-Dushman Reaction for estimating the segregation in microtubes is demonstrated in Example 4.4.

Example 4.4: Characterization of mixing in microchannel reactors.

Estimate the segregation index using the method based on Villermaux-Dushman reaction to characterize mixing in a continuous flow circular tube with a diameter of $d_t = 500\,\mu m$. The experimental set-up used is depicted in Figure 4.28. It consists of two continuously operating high-precision pumps to introduce the two miscible solutions to a microchannel. The connections of the microchannel with pumps and sample collector are made of transparent PTFE capillaries. To determine the pressure loss in the micromixer, pressure transducers are mounted at different locations including one on each upstream capillary and one on the downstream capillary. The downstream capillary is further attached to an online spectroscopic analysis system comprising a cuvette, a UV-VIS spectrometer, a light source, and a laptop.

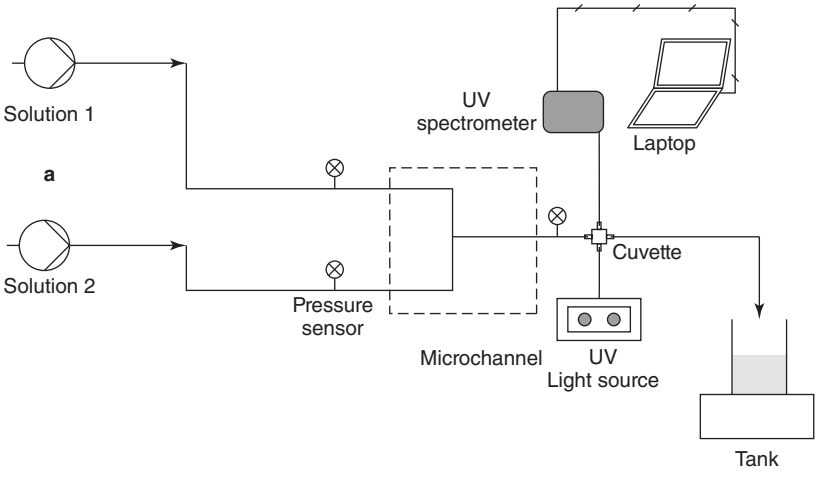

Figure 4.28 Experimental set-up for characterizing mixing in microchannels.

Table 4.2 Proposed concentration sets to be used to characterize micromixers working with two equal inlet flow rates [22].

c (kmol m^{-3})	Set 1a	Set 1b	Set 1c	Set 2a	Set 2b	Set 2c	
$[H^+]$	0.03	0.06	0.04	0.015	0.03	0.02	Solution 1
[KI]	0.032	0.032	0.032	0.016	0.016	0.016	Solution 2
$[KIO_3]$	0.006	0.006	0.006	0.003	0.003	0.003	
[NaOH]	0.09	0.09	0.09	0.045	0.045	0.045	
$[H_3BO_3]$	0.09	0.09	0.09	0.045	0.045	0.045	

Preparation of the solutions:

Acid solutions: Sulfuric acid solution is prepared from commercial concentrated solutions.

Iodide, iodate, borate solutions: First the KI and KIO_3 solutions and the H_3BO_3/NaOH buffer solutions are prepared separately. Then the iodide and iodate solutions are added to the buffer. As iodide/iodate can coexist only in basic solution; the sequence of the preparation is important to prevent the formation of iodine. In addition, oxygen should be stripped with nitrogen before use. It is also advised to prepare the solution just before the experiments.

Experimental procedure:

The two solutions are added continuously to the microchannel with identical flow rates. The formed tri-iodide is measured continuously with a UV/VIS

spectrometer. The amount of iodide formed depends on the characteristic mixing time, $t_{mx,}$ and the characteristic reaction time of the second reaction (Equation 4.38), t_{r_2}. Best results are expected for $t_{mx} \cong t_{r_2}$. Therefore, the characteristic reaction time should be adapted to the expected mixing characteristics of the micromixer. This can be done by using solutions with different reactant concentrations as summarized in Table 4.2.

The experiments were carried out at 298 K. Because of the low concentrations of the reactants, physical properties identical to water can be considered. The value of the extinction coefficient for this system is $\varepsilon_{353} = 2606\,\mathrm{m^2\,mol^{-1}}$ [64] and the optical path length is 10 mm. Using the concentration of set 2b for characterizing the microchannel ($d_t = 0.5$ mm) the following results as function of the flow rate were obtained [66]:

Flow rate, $\dot{V}$ (ml min^{-1})	4	6	8	10	12
A (–)	0.623	0.463	0.355	0.320	0.12

Solution:

The calculation is demonstrated for the first data point, and the procedure is than repeated for the remaining data. The concentration of measured component (I_3^-) from the absorbance is calculated using Equation 4.42 as

$$c_{I_3^-} = \frac{A}{\varepsilon_{353} \cdot l} = \frac{0.623}{2606 \cdot 0.01} = 0.0239\,\mathrm{mol\,m^{-3}} = 2.39 \cdot 10^{-5}\,\mathrm{mol\,l^{-1}}$$

To calculate the concentration of I_2, the equilibrium constant (Equation 4.41) is required:

$$\begin{aligned} \log_{10} K_C &= \frac{555}{T} + 7.355 - 2.575 \cdot \log_{10} T \\ &= \frac{555}{298} + 7.355 - 2.575 \cdot \log_{10} 298 = 2.846 \\ \Rightarrow K_C &= 702 \end{aligned}$$

For I_2, the quadratic equation (Equation 4.44) must be solved. Two results are obtained. But, as the equilibrium concentration of I_2 must be much smaller than the concentration of I_3^- (see Equation 4.40) the value of $c_{I_2} = 2.137 \cdot 10^{-6}\,\mathrm{mol \cdot l^{-1}}$ is correct, resulting in

$$Y = \frac{4 \cdot (c_{I_2} + c_{I_3^-})}{c_{H^+,0}} = \frac{4 \cdot (2.137 \cdot 10^{-6} + 2.39 \cdot 10^{-5})}{0.03} = 3.47 \cdot 10^{-3} \text{(Equation 4.46)}$$

The value of Y at complete segregation (Y_{CS}), eq., is given by

$$Y_{CS} = \frac{6 \cdot c_{IO_{3,0}^-}}{6 \cdot c_{IO_{3,0}^-} + c_{H_2BO_{3,0}^-}} = \frac{6 \cdot 0.003}{6 \cdot 0.003 + 0.045} = 0.286 \text{ (Equation 4.47)}$$

Thus, the segregation index is $X_s = 0.012$ for a flow rate of $\dot{V} = 4\,\text{ml} \cdot \text{min}^{-1}$. The segregation indices for all flow rates are calculated accordingly:

Flow rate, $\dot{V}$ (ml min^{-1})	4	6	8	10	12
$X_s \times 100$ (–)	1.2	0.9	0.69	0.63	0.5

The general trend in Example 4.4 shows that with increasing flow rate, the segregation index X_s decreases because of enhanced interaction between liquid elements achieving better mixing (see [27]) (Figure 4.29).

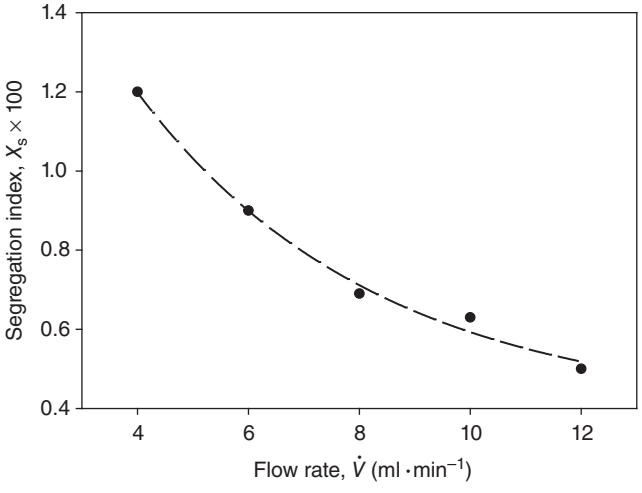

Figure 4.29 Segregation index as function of flow rate in a microchannel.

Investigation of Mixing Time The formation of iodine and in consequence the segregation index X_s in micromixers depends on the mixing time, t_{mx}, and the characteristic reaction time t_{r_2}. With the increasing ratio of $DaII_{\text{mx}} = t_{\text{mx}}/t_{r2}$ iodine yield and X_s will increase from $X_s = 0$ for $DaII_{\text{mx}} = 0$ to $X_s = 1$ for $DaII_{\text{mx}} \to \infty$ (see Section 4.1).

To estimate the mixing time from experiments, the kinetics of the second reaction (r_2) must be known allowing the calculation of t_{r_2}. In addition, a model describing the mixing process is indispensable.

Different mixing models such as the IEM (interexchange with the mean) model [67], the droplet erosion and diffusion model [68], the engulfment deformation diffusion model and the engulfment model [69, 70], and the incorporation model [71] have been proposed.

On the basis of the extensive experimental results obtained for the Villermaux-Dushman reaction, Commenge and Falk [22] elaborated a protocol for estimating the characteristic mixing time in microstructured devices. They used the IEM

model [3] to describe the mixing process. This model is considered as relatively simple. It assumes that the acid-rich zone exchanges mass with the surrounded borate-rich zone with a characteristic time constant, which corresponds to the mixing time. Plug flow behavior is considered in the microchannel, meaning that each acid-rich aggregate is in interaction with a borate-rich aggregate of the same age. The acid flow rate has a volume fraction, α, of the total flow rate, and the fraction of other inlet flow corresponds to $(1-\alpha)$. For each chemical species, there are two differential equations, one for each stream (with the subscript 1 denoting the acid-rich stream and subscript 2 the other stream) [17]:

$$\frac{dc_{i,1}}{dt} = \frac{\bar{c}_i - c_{i,1}}{t_{mx}} + R_{i,1}$$
$$\frac{dc_{i,2}}{dt} = \frac{\bar{c}_i - c_{i,2}}{t_{mx}} + R_{i,2}$$
$$\bar{c}_i = \alpha c_{i,1} + (1-\alpha)c_{i,2} \tag{4.48}$$

where $c_{i,1}$, $c_{i,2}$, and $\bar{c}_i$ are the concentrations of species i in stream 1, stream 2, and the mean concentration, respectively, while $R_{i,1}$ and $R_{i,2}$ are the transformation rates of species i in stream 1 and stream 2, respectively. These equations allow calculating the time evaluation of the different reactants in each stream by a reversible exchange between segregated regions and their mean environment through a single time constant t_{mx} and by chemical reaction in both streams.

The set of ordinary differential equations generated from Equation 4.48 can be solved for a given set of concentrations corresponding to different characteristic reaction times, t_{r_2}, and assuming a series of mixing times, t_{mx}. At the total consumption of acid, the final concentrations of iodine and tri-iodine are obtained.

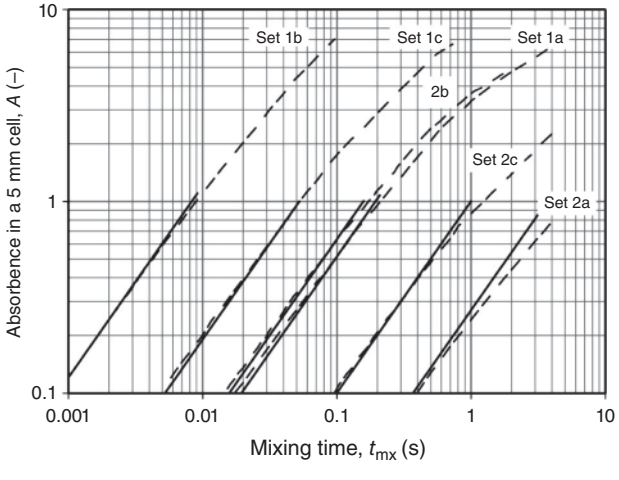

Figure 4.30 Predicted light absorbance in a 5 mm optical cell as function of mixing time and various compositions of the test solution. Model calculations: dashed lines, simplified correlation (Equation 4.49): solid lines. Results obtained for equal flow rates [22]. (Adapted with permission from Elsevier.)

This in turn can be used to calculate the light absorbance within a spectroscopic cell. The results obtained for the concentration sets summarized in Table 4.2 are plotted in Figure 4.30.

The mixing time can also be estimated with a simplified relation given in Equation 4.49.

$$t_{mx} = 0.33A' \cdot c_{H^+,0}^{-4.55} \cdot c_{I^-,0}^{-1.5} \cdot c_{IO_3^-,0}^{5.8} \cdot c_{NaOH,0}^{-2} \cdot c_{H_3BO_3,0}^{-2}$$
$$A' : \text{absorbance for an optical path length of } l = 1\,\text{mm} \tag{4.49}$$

The use of the presented relations for estimating the mixing time based on experimental data is illustrated in Example 4.5 and 4.6.

Example 4.5: Estimation of the characteristic mixing time in microchannel reactors.

Estimate the mixing time as function of the flow rate for the experiments shown in Example 4.4 and plot the mixing time as function of the power dissipation in the microchannel.

Solution:

The mixing time can be investigated using the correlation proposed in Equation 4.49. For the case of $\dot{V} = 4\,\text{ml}\,\text{min}^{-1}$ the absorbance in a cell with 10 mm optical path was found to be $A = 0.623$, which corresponds to $A' = 0.0623$ (1 mm optical path). With the concentrations of set 2b (Table 4.2) we obtain:

$$\begin{aligned} t_{mx} &= 0.33A' \cdot c_{H^+,0}^{-4.55} \cdot c_{I^-,0}^{-1.5} \cdot c_{IO_3^-,0}^{5.8} \cdot c_{NaOH,0}^{-2} \cdot c_{H_3BO_3,0}^{-2} \\ &= A' \cdot 0.33 \cdot 0.03^{-4.55} \cdot 0.016^{-1.5} \cdot 0.003^{5.8} \cdot 0.045^{-2} \times 0.045^{-2} \\ &= A' \cdot 0.7868 = 0.049\,\text{s} \end{aligned}$$

Flow rate, $\dot{V}$ ($\text{ml}\,\text{min}^{-1}$)	4	6	8	10	12
t_{mx} (s)	0.049	0.0365	0.0279	0.0252	0.0203

The specific power dissipation in a channel is given by

$$\varepsilon = \frac{\dot{V} \cdot \Delta p}{\rho \cdot V}\ (\text{W} \cdot \text{kg}^{-1})$$

The pressure drop in channels with laminar flow can be calculated with the Hagen-Poiseuille law: $\Delta p = 32\zeta \frac{\mu u}{d_h^2} L_t$ (Equation 4.22)

It follows for the specific power dissipation in circular tubes:

$$\varepsilon = \frac{\dot{V} \cdot \Delta p}{\rho \cdot V} = \frac{u \cdot \Delta p}{\rho \cdot L_t} = \frac{u \cdot 32 \cdot \mu \cdot u \cdot L_t}{\rho \cdot L_t \cdot d_h^2} = \frac{32 \cdot \nu \cdot u^2}{d_t^2}\ (\text{circular channel}) \tag{4.23}$$

With $\nu = 10^{-6}$ m^2 s^{-1}, $d_t = 0.5$ mm we obtain:

Flow rate, $\dot{V}$ (ml min^{-1})	4	6	8	10	12
ε (W kg^{-1})	14.77	33.34	59.08	92.32	132.94

The mixing time in the microchannel as a function of the specific power dissipation is shown in Figure 4.31**.** The experimental results are in good agreement with the empirical relation (Equation 4.27) shown in Figure 4.13.

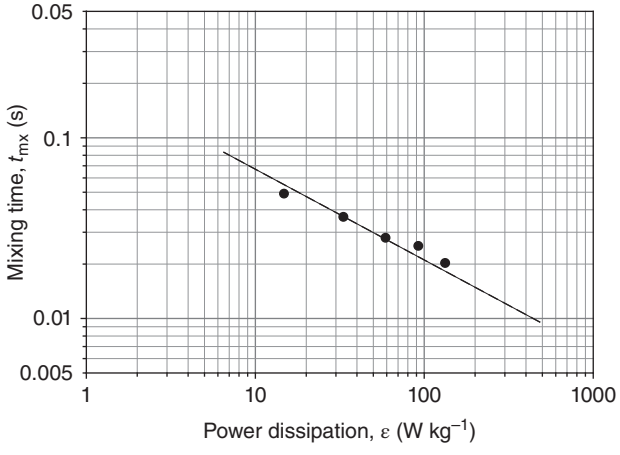

Figure 4.31 Mixing time as function of specific power dissipation. Experimental results taken from Example 4.4. Solid line: prediction with Equation 4.27.

Example 4.6: Estimation of mixing time and experimental measurements.

Commenge and Falk [22] studied a T-mixer with square channels and 90° bends. A scheme of the used mixer is shown in Figure 4.32.

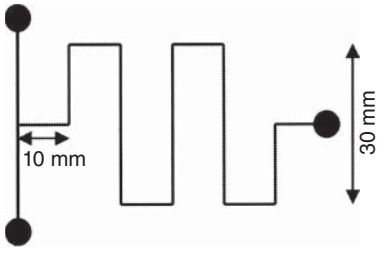

Figure 4.32 Design of the T-mixer with 10-bends.

The cross section of the channel is 1 mm wide and 1 mm deep. The total length of the channel is 180 mm and has 10 bends. Experiments were carried out at linear velocities in the range from 0.05 to 0.5 m s^{-1} corresponding to *Re* between 50 and 500. The pressure drop in the mixer is composed of two parts: the pressure drop in the square channel (Δp_s) with $d_h = 1$ mm and a length of $L_c = 180$ mm and the pressure drop in the bends (Δp_b).

The pressure drop in straight channels can be estimated with Equations 4.21 and 4.22.

$\Delta p_s = 32\zeta \frac{\mu u}{d_h^2} L_c$; with $\zeta = 0.89$ (square channels). The additional pressure drop in the bends is estimated as [22]

$$\Delta p_b = \left(1.3 + \frac{800}{Re}\right) \frac{u \cdot \rho}{2} \tag{4.50}$$

The resulting specific power dissipation lays in the range of $0.2 < \varepsilon < 20$ W kg^{-1}. With Equation 4.27 a mixing time, t_{mx} of 0.04 to 0.4 is estimated. For the experimental determination of the mixing time, a reasonable light absorbance of $0.1 < A < 2.5$ should be chosen. Regarding the predicted absorbance in a 5 mm optical cell as a function of mixing time and reactant concentrations (Figure 4.30), the use of the concentration set 1, 1c, and 2b (Table 4.2) are supposed to give reasonable experimental results under the previewed experimental conditions. The experimentally determined light absorbance as function of the *Re* in the micromixer is shown in Figure 4.33

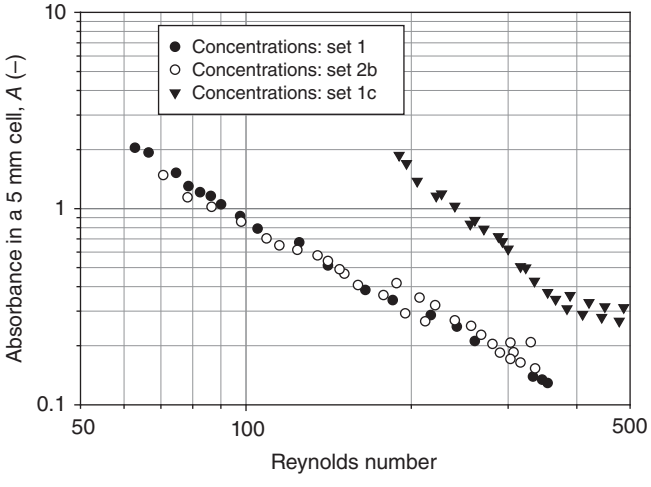

Figure 4.33 Measured absorbance, *A*, as function of *Re* for different reactant concentrations. (Values taken from Ref. [22].)

Whereas the absorbance measured with the concentration sets 1 and 2b are overlapping, the absorbance determined with set 1c are nearly 1 order of

magnitude higher. The explanation can be found in the fact that the characteristic reaction time for set 1c is considerably shorter because of the higher acid concentration. Therefore, $DaII_{mx}$ is higher at constant mixing times leading to an increasing formation of iodine and tri-iodide. On the basis of Figure 4.30 or Equation 4.49 the mixing time can be estimated and plotted as function of the *Re*. The results are shown in Figure 4.34. The mixing times determined with different reactant solutions convert to the same function. The result confirms that the iodide-iodate reaction can be used for the experimental estimation of mixing times in microstructured reactors.

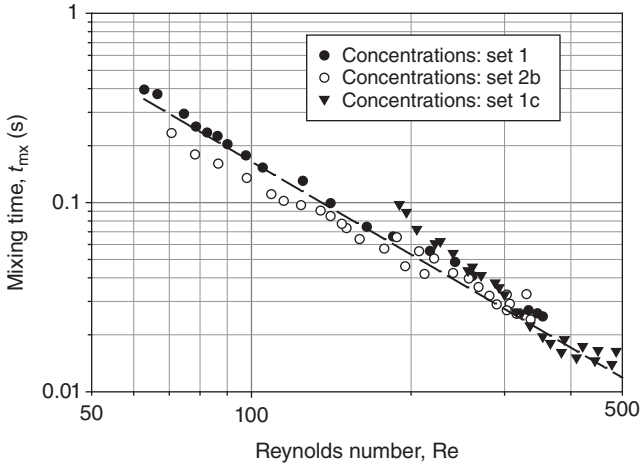

Figure 4.34 Mixing time as function of *Re* for different reactant concentrations. Dashed line corresponds to the regression line. (Values from Figure 4.33.)

4.6 Mixer Efficiency and Energy Consumption

The commonly observed trend in continuous flow micromixers is that with increasing flow velocity, that is, increasing pressure drop, mixing time decreases showing that energy input plays an important role in the rate of mixing. The energy input is expressed in terms of specific power dissipation, energy dissipation rate per unit mass of fluid, as given by Equation 4.23. The mixing time for different types of micromixers is plotted in Figure 4.13 showing a power law behavior with 30% scattering of data points and indicating that the mixing time is the function of specific power dissipation irrespective of the mixer type.

If the mixing time obtained experimentally in all micromixers is related to the specific power dissipation, the empirical relation given in Equation 4.27 is found.

By comparing it with the theoretical mixing time, the energetic efficiency of mixing (η_{mx}) can be defined as the ratio between shear rate effectively used for mixing and total shear rate used for the flow:

$$\eta_{mx} = \frac{\dot{\gamma}}{\dot{\gamma}_{max}} = \frac{\dot{\gamma}}{\sqrt{\varepsilon/(2\nu)}} \tag{4.51}$$

It is impossible to determine theoretically the value of the energetic efficiency of mixing and, therefore, the comparison of the experimental correlation (Equation 4.27) with the theoretical relation (Equation 4.26) can be used for its evaluation:

$$\eta_{mx} = \frac{\dot{\gamma}}{\dot{\gamma}_{max}} \approx \frac{t_{m,\text{theory}}}{t_{m,\exp t.}} \approx \frac{0.0075\varepsilon^{-0.5}}{0.21\varepsilon^{-0.5}} \approx 0.036 \tag{4.52}$$

It is observed that the mixing efficiency in microchannels is about 3–4%. The efficiency is even lower in conventional reactors, for example, <1% in twin-screw extruders [72]. As the mixing time is inversely proportional to the efficiency, an increase of the energetic mixing efficiency, say by a factor 3 (from 3–10%), has the same influence on the mixing time as an increase of 1 order of magnitude (10 times) power dissipation.

The reason behind such a low energetic efficiency is the mismatch of flow fields and concentration fields. The mechanical energy provided to the mixer is used to achieve the flow in device, but in zones of pure component with no interface with another component, this energy does not contribute in mixing. In the case of micromixers, multilamination improves mixing by reducing the striation thickness, but it requires additional mechanical power to create fine multilamellae before contacting.

4.7 Summary

In this chapter, theories of homogenous mixing, types of micromixers, and methods to determine characteristic mixing time have been presented. A method based on Villermaux-Dushman reaction is widely used for the efficiency characterization of different types of mixers. The wide variety of micromixers shows that the mixing can be tuned for a given chemical system using different geometries and flow rates. The choice of the device is always governed by the tradeoff between characteristic mixing time (defined by the chemical system and its intrinsic kinetics), on the one hand, and the energy consumption, on the other, indicating that energy dissipation seems to be the only relevant parameter to design an efficient mixer.

From the geometric point of view, the mixing in single-channel micromixers is not sufficient for fast reactions and, therefore, it needs to be improved further. In multilamination micromixers, the lamination improves mixing by reducing the striation thickness; however, it requires additional mechanical power to create

fine multilamellae before contacting. Besides, the zone of different concentration should be effectively contacted, so that the major part of mechanical energy supplied to the micromixer can be utilized for mixing.

4.8 List of Symbols

A, A'	Absorbance, absorbance at $l = 1$ mm	—
A'	Shape factor	—
b_s	Inverse mixing time	s^{-1}
$\bar{c}_i$,$\bar{c}_{i,L}$	Mean concentration species i, at length L	$mol\,m^{-3}$
I_s	Intensity of segregation	—
K	Flow regime parameter ($= d_h/\lambda_k$)	—
l	Thickness of the aggregate, optical path length of the spectroscopic cell	m
M	Ratio of initial concentration	—
r_d	Rate of decay	$mol^2\,m^{-6}\,s^{-1}$
$\bar{R}_i$	Overall reaction/transformation rate of partially segregated flow	$mol\,m^{-3}\,s^{-1}$
R''	Mean curve radius of the micro-channel	m
$t_{D+\text{shear}}$	Diffusion and shearing flow mixing time	s
X_S	Segregation index	—
Y, Y_{cs}	Ratio of the quantity of acid moles consumed by Villermaux–Dushman reaction, value of Y at complete segregation	—
α_i	Volume fraction of phase i	—
$\overline{\Delta c_1^2}$	Mean square of concentration fluctuations	$mol^2\,m^{-6}$
ε_i	Molar extinction coefficient at a wavelength i	$m^2\,mol^{-1}$
λ	Interface stretching factor	—
λ_K	Kolmogorov length	m
ζ_{friction}, ζ_{vortex}	Factor originating from wall friction, factor originating from both flow bending and vortex creation	—
δ	Thickness of the lamella	m
κ	Ratio of reaction rate constants	Variable
η_{mx}	Energetic efficiency of mixing/mixer	—
$\dot{\gamma}$	Shear rate	s^{-1}

References

1. Bourne, J.R. (1997) Mixing and the selectivity of fast chemical reactions, in *Handbook of Batch Process Design* (ed P.N. Sharratt), Blackie Academic & Professional.
2. Renken, A. (2006) in *Chemische Reaktoren und deren reaktionstechnische Modellierung in Technische Chemie* (eds M. Baerns, A. Behr, A. Brehm, J. Gmehling, H. Hofmann, U. Onken, and A. Renken), Wiley-VCH Verlag GmbH, Weinheim, pp. 145–194.
3. Villermaux, J. (1986) Micromixing phenomena in stirred reactors, in *Encyclopedia of Fluid Mechanics*

(eds K. Ando *et al.*), Gulf Publishing, Houston, TX.
4. Baldyga, J. and Bourne, J.R. (1999) *Turbulent Mixing and Chemical Reactions*, John Wiley & Sons, Ltd, Chichester etc.
5. Baldyga, J. (2000) Mixing and segregation in chemical reactors, in *Chemical Engineering Dynamics* (eds J. Ingham, I.J. Dunn, E. Heinzle, and J.E. Prenosil), Wiley-VCH Verlag GmbH, Weinheim.
6. Danckwerts, P.V. (1951) The definitionand measurement of some characteristics of mixing. *Appl. Sci. Res., Sect. A*, **3**, 279–296.
7. Toor, H.L. (1969) Turbulent mixing of two species with and without chemical reactions. *Ind. Eng. Chem. Fundam.*, **8** (4), 655–659.
8. Bourne, J.R. and Toor, H.L. (1977) Simple criteria for mixing effects in complex reactions. *AIChE J.*, **23** (4), 602–604.
9. Bothe, D., Stemich, C., and Warnecke, H.-J. (2006) Fluid mixing in a T-shaped micro-mixer. *Chem. Eng. Sci.*, **61** (9), 2950–2958.
10. Bothe, D., Stemich, C., and Warnecke, H.J. (2004) Theoretische und experimentelle Untersuchungen der Mischvorgänge in T-förmigen Mikroreaktoren – Teil 1: Numerische Simulation und Beurteilung des Strömungsmischens. *Chem. Ing. Tech.*, **76** (10), 1480–1484.
11. Engler, M., Kockmann, N., Kiefer, T., and Woias, P. (2004) Numerical and experimental investigations on liquid mixing in static micromixers. *Chem. Eng. J.*, **101** (1-3), 315–322.
12. Hoffmann, M., Schlüter, M., and N.R. (2006) Experimental investigation of liquid-liquid mixing in T-shaped micromixers using [mu]-LIF and [mu]-PIV. *Chem. Eng. Sci.*, **61** (9), 2968–2976.
13. Hoffmann, M., Schlüter, M., and Räbiger, N. (2007) Study of the mixing processes in microreactors by use of micro laser induced fluorescence (LIF) and micro particle imaging velocimetry (PIV). *Chem. Ing. Tech.*, **79** (7), 1067–1075.
14. Schlüter, M., Hoffmann, M., and Räbiger, N. (2004) Theoretische und experimentelle Untersuchungen der Mischvorgänge in T-förmigen Mikroreaktoren-Teil 1 Experimentelle Untersuchung des Strömungsmischens. *Chem. Ing. Tech.*, **76** (11), 1682–1688.
15. Falk, L. and Commenge, J.M. (2010) Performance comparison of micromixers. *Chem. Eng. Sci.*, **65** (1), 405–411.
16. Kockmann, N., Kiefer, T., Engler, M., and Woias, P. (2006) Convective mixing and chemical reactions in microchannels with high flow rates. *Sens. Actuators B*, **117** (2), 495–508.
17. Falk, L. and Commenge, J.-M. (2009) in *Micro Process Engineering: A Comprehensive Handbook* (eds V. Hessel, A. Renken, J.C. Schouten, and J.I. Yoshida), Wiley-VCH Verlag GmbH, Weinheim, pp. 147–173.
18. Schneider, M.A., Maeder, T., Ryser, P., and Stoessel, F. (2004) A microreactor-based system for the study of fast exothermic reactions in liquid phase: characterization of the system. *Chem. Eng. J.*, **101** (1-3), 241–250.
19. Baldyga, J. and Bourne, J.R. (1984) Mixing and fast chemical reaction-VIII: initial deformation of material elements in isotropic, homogeneous turbulence. *Chem. Eng. Sci.*, **39** (2), 329–334.
20. (2002) *VDI-Wärmeatlas*, 9 edn, Verein Deutscher Ingenieure: Springer, Berlin, Heidelberg, New York.
21. Kiwi-Minsker, L. and Renken, A. (2008) in *Handbook of Heterogeneous Catalysis* (eds G. Ertl, H. Knözinger, F. Schüth, and J. Weitkamp), Wiley-VCH Verlag GmbH, Weinheim, pp. 2248–2264.
22. Commenge, J.M. and Falk, L. (2011) Villermaux-Dushman protocol for experimental characterization of micromixers. *Chem. Eng. Proc.*, **50**, 979–990.
23. Capretto, L., W.C. , Hill, M., and Zhang, X. (2011) Micromixing within microfluidic devices. *Top. Curr. Chem.*, **304**, 27–68.
24. Kumar, V., Paraschivoiu, M., and Nigam, K.D.P. (2011) Single-phase fluid flow and mixing in microchannels. *Chem. Eng. Sci.*, **66**, 1329–1373.
25. Hessel, V., Hofmann, C., Löwe, H., Meudt, A., Scherer, S., Schönfeld, F., and Werner, B. (2004) Selectivity gains and energy savings for the industrial phenyl boronic acid process

using micromixer/tubular reactors. *Org. Process Res. Dev.*, **8** (3), 511–523.
26. Löwe, H., Ehrfeld, W., Hessel, V., Richter, T., and Schiewe, J. (2000) Micromixing technology. 4th International Conference on Microreaction Technology (IMRET4), Atlanta, GA, 2000, pp. 31–47.
27. Kashid, M., Renken, A., and Kiwi-Minsker, L. (2011) Mixing efficiency and energy consumption for five generic microchannel designs. *Chem. Eng. J.*, **167** (2-3), 436–443.
28. Jiang, F., Drese, K.S., S.H. , Kupper, M., and Schonfeld, F. (2004) Helical flows and chaotic mixing in curved micro channels. *AIChE J.*, **50** (9), 2297–2305.
29. Mengeaud, V., Josserand, J., and Girault, H.H. (2002) Mixing processes in a zigzag microchannel: finite element simulations and optical study. *Anal. Chem.*, **74** (16), 4279–4286.
30. Kölbl, A., Kraut, M., and Wenka, A. (2011) Design parameter studies on cyclone type mixers. *Chem. Eng. J.*, **167** (2-3), 444–454.
31. Ansari, M.A., Kim, K.-Y., Anwar, K., and Kim, S.M. (2012) Vortex micro T-mixer with non-aligned inputs. *Chem. Eng. J.*, **181–182**, 846–850.
32. Hessel, V., Lowe, H., and Schonfeld, F. (2005) Micromixers – a review on passive and active mixing principles. *Chem. Eng. Sci.*, **60** (8-9), 2479–2501.
33. Schönfeld, F., Hessel, V., and Hofmann, C. (2004) An optimised split-and-recombine micro-mixer with uniform 'chaotic' mixing. *Lab Chip*, **4** (1), 65–69.
34. Jen, C.-P., Wu, C.-Y., Lin, Y.-C., and Wu, C.-Y. (2003) Design and simulation of the micromixer with chaotic advection in twisted microchannels. *Lab Chip*, **3** (2), 77–81.
35. Bertsch, A., Heimgartner, S., Cousseau, P., and Renaud, P. (2001) Static micromixers based on large-scale industrial mixer geometry. *Lab Chip*, **1** (1), 56–60.
36. Stroock, A.D., Dertinger, S.K.W., Ajdari, A., Mezić, I., Stone, H.A., and Whitesides, G.M. (2002) Chaotic mixer for microchannels. *Science*, **295** (5555), 647–651.
37. Stroock, A.D. and McGraw, G.J. (2004) Investigation of the staggered herringbone mixer with a simple analytical model. *Philos. Trans. R. Soc. London, Ser. A*, **362** (1818), 971–986.
38. Choudhary, R., Bhakat, T., Singh, R.K., Ghubade, A., Mandal, S., Ghosh, A., Rammohan, A., Sharma, A., and Bhattacharya, S. (2011) Bilayer staggered herringbone micro-mixers with symmetric and asymmetric geometries. *Microfluid. Nanofluid.*, **10** (2), 271–286.
39. Werner, B., Donnet, M., Hessel, V., Hofmann, C., Jongen, N., Lowe, H., Schenk, R., and Ziogas, A. (2002) Specially suited micromixers for process involving strong fouling. 6th International Conference on Microreaction Technology, IMRET 6, AIChE, New Orleans, 2002, pp. 168–183.
40. Penth, B. (2001) Method and device for carrying out chemical and physical processes. WO Patent 2000061275 A3.
41. Song, H., Tice, J.D., and Ismagilov, R.F. (2003) A microfluidic system for controlling reaction networks in time. *Angew. Chem. Int. Ed.*, **42** (7), 768–772.
42. Matsuyama, K., Tanthapanichakoon, W., Aoki, N., and Mae, K. (2007) Operation of microfluidic liquid slug formation and slug design for kinetics measurement. *Chem. Eng. Sci.*, **62** (Special Issue 18-20), 5133–5136.
43. Bringer, M.R., Gerdts, C.J., Song, H., Tice, J.D., and Ismagilov, R.F. (2004) Microfluidic systems for chemical kinetics that rely on chaotic mixing in droplets. *Philos. Trans. R. Soc. London, Ser. A*, **362** (1818), 1087–1104.
44. Paik, P., Pamula, V.K., and Fair, R.B. (2003) Rapid droplet mixers for digital microfluidic systems. *Lab Chip*, **3** (4), 253–259.
45. Seidel, R.U., Sim, D.Y., W.M. , and Esashi, M. (2000) *Third International Conference on Microreaction Technology. IMRET 3*, Springer, Berlin, pp. 189–197.
46. Hong, C.-C., Choi, J.-W., and Ahn, C.H. (2004) A novel in-plane passive microfluidic mixer with modified tesla structures. *Lab Chip*, **4** (2), 109–113.
47. Hong, C.-C., Choi, J.-W., and Ahn, C.H. (2001) in *Micro Total Analysis Systems* (eds J.M. Ramsey and A. van den Berg),

Kluwer Academic Publishers, Dordrecht, pp. 31–33.
48. Yasui, T., Omoto, Y., Osato, K., Kaji, N., Suzuki, N., Naito, T., Watanabe, M., Okamoto, Y., Tokeshi, M., Shamoto, E., and Baba, Y. (2011) Microfluidic baker's transformation device for three-dimensional rapid mixing. *Lab Chip*, **11** (19), 3356–3360.
49. Voldman, J., Gray, M.L., and Schmidt, M.A. (1998) in *Micro Total Analysis Systems* (eds J. Harrison and A. van den Berg), Kluwer Academic Publishers, Dordrecht, pp. 181–184.
50. Glasgow, I. and N.A. (2003) Enhancement of microfluidic mixing using time pulsing. *Lab Chip*, **3** (2), 114–120.
51. Niu, X.Z. and Lee, Y.K. (2003) Efficient spatial-temporal chaotic mixing in microchannels. *J. Micromech. Microeng.*, **13** (3), 454–462.
52. Qian, S.Z. and Bau, H.H. (2002) A chaotic electroosmotic stirrer. *Anal. Chem.*, **74** (15), 3616–3625.
53. Oddy, M.H., Santiago, J.G., and Mikkelsen, J.C. (2001) Electrokinetic instability micromixing. *Anal. Chem.*, **73** (24), 5822–5832.
54. Yang, Z., Goto, H., Matsumoto, M., and Maeda, R. (2000) Active micromixer for microfluidic systems using lead-zirconate-titanate(PZT)-generated ultrasonic vibration. *Electrophoresis*, **21** (1), 116–119.
55. Woias, P., Hauser, K., and Yacoub-George, E. (2000) in *Micro Total Analysis Systems* (eds A. van den Berg, W.O. , and P. Bergveld), Kluwer Academic Publishers, Dordrecht, pp. 277–282.
56. Liu, R.H., Yang, J., Pindera, M.Z., Athavale, M., and Grodzinski, P. (2002) Bubble-induced acoustic micromixing. *Lab Chip*, **2** (3), 151–157.
57. Liu, R.H., Lenigk, R., Druyor-Sanchez, R.L., Yang, J., and Grodzinski, P. (2003) Hybridization enhancement using cavitation microstreaming. *Anal. Chem.*, **75** (8), 1911–1917.
58. Lu, L.-H., Ryu, K.S., and Liu, C. (2000) A magnetic microstirrer and array for microfluidic mixing. *J. Microelectromech. Syst.*, **11** (5), 462–469.
59. West, J., Karamata, B., Lillis, B., Gleeson, J.P., Alderman, J., Collins, J.K., Lane, W., Mathewson, A., and Berney, H. (2002) Application of magnetohydrodynamic actuation to continuous flow chemistry. *Lab Chip*, **2** (4), 224–230.
60. Bourne, J.R. and Yu, S. (1994) Investigation of micromixing in stirred tank reactors using parallel reactions. *Ind. Eng. Chem. Fundam.*, **33** (1), 41–55.
61. Bourne, J.R., Kut, O.M., Lenzner, J., and Maire, H. (1990) Kinetics of the diazo coupling between 1-naphthol and diazotized sulfanilic acid. *Ind. Eng. Chem. Fundam.*, **29** (9), 1761–1765.
62. Baldyga, J., Bourne, J.R., and Walker, B. (1998) Non-isothermal micromixing in turbulent liquids: theory and experiment. *Can. J. Chem. Eng.*, **76** (3), 641–649.
63. Holvey, C.P., Roberge, D.M., Gottsponer, M., N.K. , and Macchi, A. (2011) Pressure drop and mixing in single phase microreactors: simplified designs of micromixers. *Chem. Eng. Proc.*, **50** (10), 1069–1075.
64. Guichardon, P. and Falk, L. (2000) Characterisation of micromixing efficiency by the iodide-iodate reaction system. Part I: Experimental procedure. *Chem. Eng. Sci.*, **55** (19), 4233–4243.
65. Guichardon, P. and Falk, L. (2000) Characterisation of micromixing efficiency by the iodide-iodate reaction system. Part II:kinetic study. *Chem. Eng. Sci.*, **55** (19), 4245–4253.
66. Kumar, A. (2012) Characterization of Hot Spots in Microstructured Reactors for Fast and Exothermic Reactions in Mixing Regime, Ecole Polytechnique Fédérale de Lausanne, EPFL, Lausanne.
67. Villermaux, J. and Devillon, J.C. (1972) Représentation de la coalescence et de la redispersion des domaines de ségrégation dans un fluide par un modéle d'interaction phénoménologique. 2nd International Symposium on Chemical Reaction Engineering, Amsterdam, The Netherlands, 1972.
68. Ou, J.J. and Ranz, W.E. (1983) Mixing and chemical reactions. Chemical selectivities. *Chem. Eng. Sci.*, **38** (7), 1015–1019.
69. Baldyga, J. and Bourne, J.R. (1990) Comparison of the engulfment and the

interaction-by-exchange-with-the-mean micromixing models. *Chem. Eng. J.*, **45** (1), 25–31.

70. Baldyga, J. and Bourne, J.R. (1989) Simplification of micromixing calculations. I. Derivation and application of new model. *Chem. Eng. J.*, **42** (2), 83–92.

71. Fournier, M.C., Falk, L., and Villermaux, J. (1996) A new parallel competing reaction system for assessing micromixing efficiency-determination of micromixing time by a sample mixing model. *Chem. Eng. Sci.*, **51** (23), 5187–5192.

72. Baldyga, J., Rozen, A., and Mostert, F. (1998) A model of laminar micromixing with application to parallel chemical reactions. *Chem. Eng. J.*, **69** (1), 7–20.